INVESTIGATION OF ODE-BASED NON-EQUILIBRIUM WALL SHEAR STRESS MODELS FOR LARGE EDDY SIMULATION

A Thesis
Presented to
The Academic Faculty

By

Tarik Dzanic

In Partial Fulfillment
of the Requirements for the Degree
Master of Science in the
School of Aerospace Engineering

Georgia Institute of Technology

August 2019

INVESTIGATION OF ODE-BASED NON-EQUILIBRIUM WALL SHEAR STRESS MODELS FOR LARGE EDDY SIMULATION

Approved by:

Professor Joseph Oefelein, Advisor
School of Aerospace Engineering
Georgia Institute of Technology

Professor Suresh Menon
School of Aerospace Engineering
Georgia Institute of Technology

Professor P.K. Yeung
School of Aerospace Engineering
Georgia Institute of Technology

Date Approved: July 24, 2019

ACKNOWLEDGEMENTS

I would like to thank my advisor Professor Joseph Oefelein and my committee members, Professor Suresh Menon and Professor P.K. Yeung, for their help on this work. I would also like to thank Semir Sarajlic and the people at PACE with their immense help in resolving my issues on the computing clusters.

TABLE OF CONTENTS

LIST OF TABLES

LIST OF FIGURES

LIST OF SYMBOLS

α	Ratio of friction velocity to modified inner velocity
B	Law of the wall constant
$\overline{\beta}$	Complement of the average α value in the wall model region
c	Chord length
c_i	Polynomial interpolation coefficients
C_f	Skin friction coefficient
C_p	Pressure coefficient
C_s	Smagorinsky coefficient
δ	Boundary layer height
Δ	LES filter width
F	Forcing function
h_{wm}	Wall model height
κ	Von Karman constant
M	Mach number
μ	Dynamic viscosity
μ_t	Dynamic turbulent eddy viscosity
ν	Kinematic viscosity
ν_t	Kinematic turbulent eddy viscosity
Φ	Hyperbolic tangent smoothing function
ρ	Density
R	Overprediction factor
Re	Reynolds number
σ_{ij}	Shear stress tensor
S_{ij}	Strain-rate tensor
t	Time

τ_{ij}^R	Residual stress tensor
τ_w	Wall shear stress
$\tau_{w(wm)}$	Wall model wall shear stress
u	Wall parallel velocity
u_f	Forcing velocity
$u_{f\tau}$	Modified inner velocity
u_τ	Friction velocity
U^*	Modified nondimensional velocity
U_∞	Freestream velocity
y^+	Nondimensional wall distance
y^*	Modified nondimensional wall distance

SUMMARY

For high Reynolds number flows, wall modeling is essential for performing large eddy simulation at a reasonable computational cost. In this work, a novel low-cost ODE-based non-equilibrium wall model is introduced for wall shear stress modeling in LES. Using polynomial approximations of the pressure gradient and convective terms obtained from interpolation of the LES solution, as opposed to direct evaluation of these gradients within the wall model, the governing wall model equations reduce from coupled PDEs to uncoupled ODEs that do not require an embedded wall model grid within the LES grid. Additionally, the steady form of the wall model equations was utilized, feasible due to the spatial decoupling of the wall model equations, and the effects of the temporal evolution on the wall shear stress were modeled. The effects of polynomial degree on the accuracy of the wall shear stress predictions were explored, and an empirical lag model was built to model the unsteady effects without requiring the solution of a time-stepping problem. Wall resolved large eddy simulations of separated flow around the NASA wall mounted hump and an iced NACA 63A213 airfoil were performed and used as a reference for the comparison of the non-equilibrium wall model to a commonly used equilibrium wall model. The proposed non-equilibrium wall model was able to predict separated flow and laminar flow regions in much better agreement with the wall resolved results than the equilibrium wall model. Underpredictions in the skin friction coefficient in non-equilibrium flow regimes were reduced from 20-50% to less than 10% between the equilibrium and the non-equilibrium wall modeled approaches. Minor improvements in the pressure coefficient predictions were observed with the non-equilibrium model in the separated flow region of the iced airfoil. The results suggest that the proposed wall model can offer better predictions of separated and/or laminar flows compared to equilibrium wall models with negligible computational cost increase.

CHAPTER 1
INTRODUCTION

It is well known that the nonlinear multi-scale nature of turbulence makes the computational cost of large eddy simulation (LES) prohibitive at high Reynolds numbers. This is particularly true for wall bounded flows since the length scales within the inner boundary layer get progressively smaller with increasing Reynolds number whereas the outer flow length scales are nearly independent. To adequately resolve the inner boundary layer, the grid resolution must scale with the viscous length scale, which is infeasible for many engineering applications. Therefore, for high Reynolds numbers, it is preferable to resolve only the outer boundary layer and model the inner boundary layer. For this approach; i.e., wall modeled LES (WMLES), the grid resolution scales with the boundary layer thickness instead of the viscous length scale [1]. As such, the number of grid points in WMLES can be one to three orders of magnitude less than wall resolved LES (WRLES). Paired with the significantly larger computational time step possible on this coarser grid, it is clear why WMLES is of practical importance to applications with wall bounded flows at high Reynolds numbers.

The approach for WMLES generally falls within one of two categories: (1) methods that attempt to predict the wall shear stress τ_w directly, and (2) methods that switch to a Reynolds-Averaged Navier-Stokes (RANS) formulation within the inner boundary layer. Although both methods are able to predict the wall shear stress accurately to within $5 - 15\%$ in canonical boundary layer flows, a mismatch in the predicted velocity profile in the logarithmic layer plagues both methods, albeit for different reasons, and prevents more accurate predictions of wall shear stress [2]. This is of particular importance for more complex flows with separation since the predicted point of separation is dependent on the state of the upstream boundary layer, which is dependent on the upstream wall shear stress.

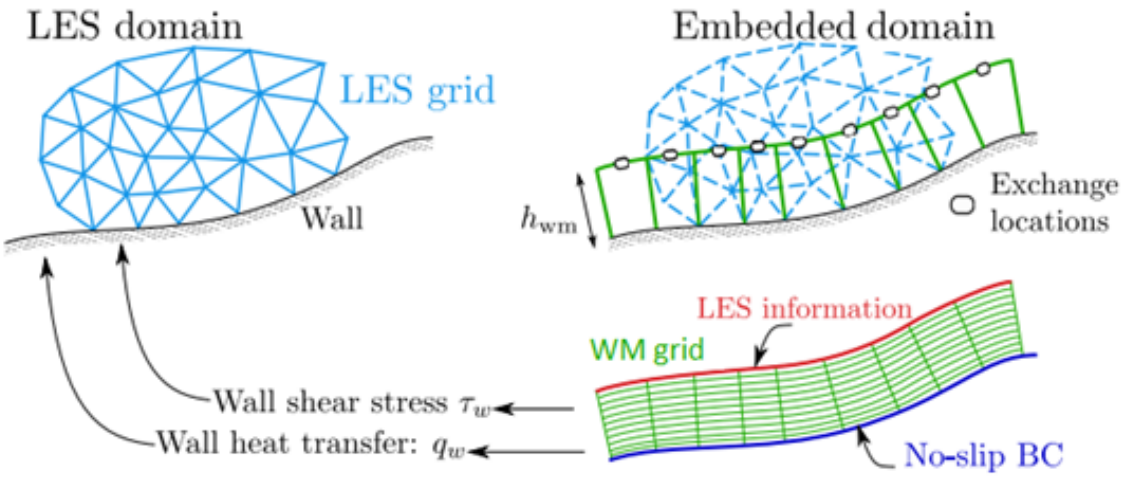

Figure 1.1: Schematic of the wall shear stress modeling approach [3].

The objective of this work is to explore the method of predicting the wall shear stress directly. For this approach, the grid is not resolved well enough to accurately predict the wall shear stress with a no-slip boundary condition. Instead, the wall model predicts the wall shear stress based on the LES solution at some height h_{wm} above the wall (the wall model height). The framework of this method is shown in the schematic in Figure 1.1. The wall model equations are solved by enforcing the no-slip condition at the wall and matching the LES velocity u_{LES} (and temperature, if required) at a given wall model height h_{wm}. This height is generally set at several grid points away from the wall since, as shown by Kawai & Larsson, input from the LES solver at the first grid point is not well enough resolved to yield accurate predictions of the wall shear stress [2]. The calculated wall shear stress τ_w (and heat flux, if required) from the wall model solution is then fed back to the LES solver as a Neumann boundary condition.

1.1 Wall Shear Stress Modeling: History

Initial attempts of near wall modeling originated as approximate boundary conditions. In 1970, Deardorff attempted to perform large eddy simulation of a channel flow on a sig-

nificantly underresolved grid due to the computing power at the time. He matched the wall normal second derivative of the velocity to the log law values, which yielded poor results [4]. Subsequently in 1975, Schumann modified this approach and introduced the method now commonly known as wall shear stress modeling [5]. For a similar channel flow, as well as annular flows, Schumann attempted to model the effects of the near wall turbulence by applying boundary conditions for the wall parallel velocity derivative instead of the no-slip condition. Using known values of the mean wall shear stress and velocity, he modeled the instantaneous wall shear stress as the product of the mean stress ($< \tau_w >$) and the ratio of the instantaneous velocity (u_1) to the mean velocity ($< u_1 >$) at the first cell as

$$\tau_w(x,z) =< \tau_w(x,z) > \frac{u_1(x,z)}{< u_1(x,z) >}. \tag{1.1}$$

This model resulted in notable improvements over the underresolved no-slip condition, and showed that for underresolved grids, the method of applying the wall shear stress as a boundary condition was sufficient to model the near wall effects.

Developments beyond these early works were initially constrained to algebraic models based on the law of the wall due to constraints in computational power. Grötzbach modified the method of Schumann by using the instantaneous fit of the log-law velocity profile, and further improvements were made by Piomelli *et al.* to account for the various effects of tilting of eddies and bursts near the wall [6, 7]. These methods assume that the near-wall velocity profile can be approximated by the log-law, given as

$$\frac{u}{u_\tau} = \frac{1}{\kappa} ln\Big(\frac{y u_\tau}{\nu}\Big) + B, \qquad u_\tau = \sqrt{\tau_w/\rho}. \tag{1.2}$$

where τ_w denotes the wall shear stress, u_τ the friction velocity, $\kappa \approx 0.41$ the von Karman constant, and $B \approx 5$. This approximation includes the assumptions of incompressible flow with no pressure gradients and the interface between the LES solver and the wall model is within the log-layer. Generalizations of this profile can be extended to compressible flows

using Van Driest transformations. Further generalizations of this algebraic wall model were performed by Shih *et al.* for flows with pressure gradients and for interfaces within the viscous sublayer and buffer layer [8]. Alternative approaches based on power law representations have been investigated (e.g., Werner and Wengle [9]), which do not produce significantly different results.

A different approach approximating the wall shear stress is based on modeling fluctuations. For simple flows, where the mean velocity and wall shear stress are known a priori, the fluctuations in the wall shear stress can be modeled by assuming they are proportional to fluctuations in the near wall velocity [6]. This approach was generalized by Wu and Squires by using a steady-state RANS solution near the wall to determine the mean velocity and shear stress, and then applying the fluctuations as mentioned, with moderate improvements [10]. However, this approach is limited by the accuracy of the method used to obtained the mean quantities, and as such is susceptible to the drawbacks of RANS methods.

Although algebraic law of the wall models are attractive due to their low computational cost, their assumptions are heavily constrained. For many complex flows, such as those involving separation or transition, the velocity profile does not obey the law of the wall. Accurate prediction of the wall shear stress for a broader range of flows requires more detailed models. Such models are typically based on the boundary layer equations.

Initial work based on boundary layer equation wall modeling was performed by Hoffman and Benocci in 1995 [11]. Using an algebraic turbulence model, they integrated the unsteady boundary layer equations analytically to calculate the wall shear stress. Results using this approach were in good agreement with wall resolved LES and experimental data of a channel flow, indicating that the boundary layer equation method was a viable option for near wall modeling. This approach was extended by Wang in 1999 to simulate aeroacoustic effects over the trailing edge of an airfoil, with and without the pressure gradient term [12]. Good predictions of the wall shear stress were obtained for regions of the flow

where the pressure gradient was favorable or zero. However, poor results in both the wall shear stress and pressure fluctuations were obtained in regions where the pressure gradient was adverse. These collective observations laid the foundation for the most common method in wall shear stress modeling used presently called "the zonal approach."

1.2 Zonal Approaches

Zonal approaches use a separate set of equations near the wall, either through use of a separate grid, known as the Two-Layer Method (TLM), or through the use of a single grid with a change in the turbulence model, known as Detached Eddy Simulation (DES). The latter is classified under hybrid-RANS/LES methods and is outside the scope of this work. The TLM was introduced by Balaras and Benocci in 1994, and subsequently improved in 1996, and is the basis for most modern wall modeled approaches presently [13, 14]. This method uses an inner grid embedded within the LES grid near the wall that is only refined in the wall normal direction. Within this inner grid, simplified versions of the governing flow equations are solved with the assumption that the interactions between the inner and outer flow regions are weak.

The TLM proposed by Balaras and Benocci uses the full thin boundary layer equations (TBLE), given as

$$\frac{\partial u_i}{\partial t} + u_j \frac{\partial u_i}{\partial x_j} + \frac{1}{\rho}\frac{\partial P}{\partial x_i} = \frac{\partial}{\partial x_n}\left[(\nu + \nu_t)\frac{\partial u_i}{\partial x_n}\right] \tag{1.3}$$

where n denotes the wall normal direction, i denotes the wall parallel directions, $j = 1, 2, 3$, and ν_t is an algebraic "Smagorinsky-like" turbulent eddy viscosity with near wall damping. Boundary conditions were applied to enforce the no-slip condition at the wall and the LES velocity at the first grid point. This approach was applied to a channel flow at varying Reynolds numbers as well as flow in a square duct and a rotating channel. For the channel flow, the results did not differ much from the algebraic approach of Schumann. However, for the latter two flows, due to the presence of secondary flows which deviate significantly

from the log-law, the TLM showed significant improvements over the algebraic models, in good agreement with DNS and experiments.

The TLM has been the subject of many studies in subsequent years for flows such as a backward-facing step and an airfoil trailing edge [15, 16, 17]. Results have demonstrated that solving the TBLE explicitly results in more accurate predictions of the wall shear stress and flow dynamics compared to algebraic representations of the law of the wall. Most recently, the TLM has evolved into two distinct methods of wall modeling within the community: non-equilibrium and equilibrium models. The principle of momentum conservation in a nearly parallel shear flow is the basis for both of these approaches. The treatment of the left-hand side terms of Eq. (1.3) dictates how these models are segregated.

1.2.1 Non-Equilibrium Wall Models

Similar to the original TLM, non-equilibrium models retain all of the terms on left hand side. Within the wall model layer, the unsteady TBLE for both wall parallel momentum components are solved with updated boundary conditions from the LES solver at each time step. Wall parallel derivatives are evaluated for both the pressure gradient and convective terms. Many wall models make the assumption that the pressure gradient does not vary in the wall normal direction within the wall model region, and therefore can be imposed for the outer LES solution [18, 3]. No assumptions on variations of the wall parallel derivatives for the convective terms are made. Thus, these must be evaluated within the wall region.

Since the governing equations for non-equilibrium models are explicitly defined, research efforts have been focused on other issues. A notable improvement over the original TLM was made by Wang and Moin in 2002 [17]. They found that the inclusion of the convective terms carries some of the unresolved shear stress, and therefore the eddy viscosity must be lowered to account for that. The eddy viscosity was scaled to match the LES eddy viscosity at the interface location, lowering it by roughly a factor of 2. This approach yielded significantly better results for the previously attempted airfoil trailing edge in terms

of predicted wall shear stress, separation, and lower-order velocity statistics. Further improvements of this model were introduced by Kawai and Larsson in 2013 [2], where they reasoned that the eddy viscosity scaling parameter was not independent of wall distance, as assumed by Wang and Moin. This resulted in a Reynolds number dependency on the accuracy of the wall shear stress prediction. It was shown that a large change in the ratio of resolved and unresolved shear stresses is present in the wall normal direction, and therefore the eddy viscosity scaling parameter should vary accordingly. Thus, Kawai and Larsson used the original scaling parameter values near the wall, and decreased them in a quadratic fashion to match the LES eddy viscosity moving away from the wall, which resulted in significantly better predictions of shock-boundary layer interactions.

1.2.2 Equilibrium Wall Models

In the equilibrium wall model approach, the pressure gradient, time derivative, and convective terms are assumed to balance exactly, such that the left-hand side of Eq. (1.3) is zero. Additionally, the flow within the wall model region is assumed to be parallel to the wall and in-plane, such that a single wall-parallel momentum equation can be used. This reduces the system of coupled PDEs to a single steady ODE in the wall normal direction. Although the equilibrium assumption is insufficient for non-equilibrium flows, it is not as restrictive as it might appear since there is a physical relation between the pressure gradient and convective terms in the momentum equation. Adverse pressure gradients result in flow deceleration, and vice versa. Thus, although these terms might be of non-negligible magnitude in non-equilibrium flows, their sum should be approximately zero above the viscous sublayer [18, 19]. Mathematically, it can be shown that above the viscous sublayer in the limit of vanishing viscosity, integration of the boundary layer equations along a streamline reduces to the Bernoulli equation [3]. Therefore, even for non-equilibrium flows, the near-wall equilibrium assumption is not necessarily ill-posed (i.e., see for example the wall modeled simulations of shock boundary layer interactions by Bermejo-Moreno *et al.* [20]).

1.2.3 Equilibrium versus Non-Equilibrium Models: Advantages and Disadvantages

A comparison of the equilibrium and non-equilibrium modeling approaches can be performed for three metrics: accuracy, computational cost, and complexity.

Accuracy

For equilibrium flows (i.e. flows without large pressure gradients or separation), the near-wall equilibrium assumption is well-posed. Numerous numerical studies have been performed with the equilibrium model for these flows with good results [21, 22, 23, 24]. Likewise, for flows with mild non-equilibrium effects, equilibrium models still perform well owing to the reasoning for the equilibrium assumption previously stated. However, non-equilibrium models are noteably more accurate in flows with: (1) strong separation, and/or (2) laminar regimes. For flows with strong separation, the assumption that the pressure gradient matches the convective term does not hold as well and inflections in the velocity profile within the wall model region cannot be captured by equilibrium models since their solution is monotonic. For laminar flows, viscous and pressure gradient effects are dominant in comparison to the convective term and therefore can be more accurately resolved by non-equilibrium wall models [25]. These two cases are shown in Figure 1.2 for instantaneous flow over an iced airfoil with contours of the sum of the pressure gradient and convective terms. Over the upper surface the flow is strongly separated. Over the lower surface the flow is laminar. Within the wall model region, outlined in white, many instances of a nonzero sum are observed. Therefore, wall models that include the non-equilibrium effects are potentially more accurate for a broader range of flows compared to equilibrium wall models [25, 26, 27].

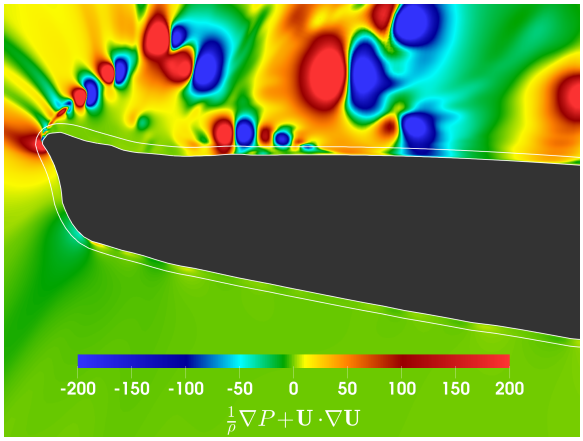

Figure 1.2: Instantaneous non-equilibrium terms nondimensionalized by the freestream velocity and chord length in flow over an iced airfoil in stall with the wall model height outlined in white.

Computational Cost

There is a large difference in computational cost between equilibrium and non-equilibrium models. For equilibrium models, a nonlinear one-dimensional boundary value problem must be solved for each wall surface cell. This is generally done numerically and iteratively, although some analytic equilibrium models exist. As a result, the overall computational cost of an equilibrium wall model can be up to 30% of the LES solution per time step. In comparison, non-equilibrium wall models have to solve a time-stepping problem within the wall model, which is much cheaper to solve per time step in comparison to the nonlinear one-dimensional boundary value problem of the equilibrium wall model. However, by solving a time-stepping problem on the wall model grid, the LES solver must abide by the CFL constraints of the wall model solution. The minimum grid spacing within the non-equilibrium wall model grid can be one to two orders of magnitude smaller than the wall model height. Thus, severe time step restrictions must typically be applied to the LES solver [18]. Even with the smaller computational cost per time step to solve the non-equilibrium equations, the overall cost due to the decreased time step can be multiple times the cost of an LES solution with an equilibrium wall model.

Attempting to remove the CFL constraints of non-equilibrium wall models by neglecting or modeling the time derivative and treating the equations as a boundary value problem results in an even more computationally difficult problem. This is due to the coupling caused by the wall parallel derivatives. The domain of the boundary value problem must not only span the wall model height in the wall normal direction (as in equilibrium wall models), but also along the entire wall surface, which results in a nonlinear three dimensional boundary value problem. Paired with the iterative solution technique required of this type of nonlinear problem, the computational cost of a non-equilibrium wall model without the time derivative would be orders of magnitude higher than one with the term included. Thus, potential improvements in the computational cost of non-equilibrium models can be obtained if the solutions are decoupled and the time derivative is neglected. This is the basis of this work, as outlined in Sections 1.3 and 1.4.

Complexity

Between the two methods, the complexity of implementation varies significantly. For the equilibrium approach, only the LES solution at the wall model height above each wall grid point is required to solve the wall shear stress. Once the wall shear stress is calculated, the current wall model solution does not need to be stored. Additionally, since there is no dependence on the adjacent wall model solutions, calculating the wall shear stress can be done extremely efficiently in parallel. For the non-equilibrium approach, an embedded grid must be generated near the wall. For structured solvers, this does not pose much of a problem since the first LES cell can be refined in the wall normal direction to the desired resolution. However, for complex geometries and unstructured solvers, generating this near wall grid can be a tedious task. Parallelization also becomes more difficult since the wall model must exchange information in between adjacent cells and the LES solver.

In summary, the computational cost and complexity of equilibrium wall models is notably less than non-equilibrium wall models and can provide accurate results for many types of flows. However, non-equilibrium wall models have been shown to be more accurate for a broader range of flows. In particular, non-equilibrium wall models are generally more robust and widely applicable for complex flows with separation or locally laminar regimes, albeit at a significantly higher computational cost and complexity.

1.3 Development of Approximate Non-Equilibrium Wall Models

Given the observations above, it is beneficial to consider wall models that treat the non-equilibrium terms while only requiring the solution of ODEs in the wall normal direction to maintain optimal computational efficiency. In recent years, efforts have been focused on developing these approximate ODE-based non-equilibrium wall models, with particular emphasis placed on modeling the convective term since the pressure gradient term is generally constant within the wall model region. Hickel *et al.* [18] first attempted to model the convective term as a function of the velocity to some power, which resulted in poor predictions of the wall shear stress when using the LES solution at the wall model height. Their second attempt used a linear convective term profile that matched the pressure gradient at the wall model height and decreased linearly to zero at the wall. This approximation gave better results, but the approximation that the convective term matches the pressure gradient term at the wall model height introduced unnecessary errors since the convective term is evaluated by the LES solver and should be used as the matching condition instead. Another attempt by Yang *et al.* [28] used a parametric shape function for the velocity and analytically integrated the momentum equation within the wall model region by matching the LES solution with reasonable results. However, this integral method relies on the assumption that the velocity profile can be represented by the chosen shape functions (i.e. profiles with logarithmic and linear regions), which can be ill-posed for separated flows.

In both of these works, the wall model solution is treated as a time stepping problem since the inclusion of the convective term without the time derivative is not physically consistent. Additionally, neglecting the time derivative results in elliptic governing equations. The solution of these equations can lead to erroneous over-predictions of the wall shear stress in comparison to equations that include the time derivative since the changes in the LES solution are instantaneously propagated throughout the wall model solution [11, 29]. However, significant improvements in the computational cost can be obtained if the time derivative is neglected. Just like the approximation of the convective terms, the non-equilibrium wall model equations will then become spatially decoupled into one dimensional domains like the equilibrium wall model approach.

To maintain physical consistency and reduce the errors in the wall shear stress prediction due to neglecting the time derivative, the effects of the temporal evolution of the flow must be accounted for. Research into modeling the temporal evolution within the wall model region is currently very sparse since equilibrium models neglect the time derivative and "exact" non-equilibrium models suffer a large computational cost increase from neglecting this term. Some insight can be gained from early works in wall shear stress modeling that use analytic formulations, particularly by Hoffmann and Benocci in 1995 [11]. In this work, they did not solve the unsteady boundary layer equations but accounted for the time derivative. For attached turbulent flows, they showed that the bulk time derivative can be approximated well using the time derivative of the LES velocity at the wall model height scaled by the ratio of the wall model velocity to the LES velocity. However, for flows where the velocity gradients at the wall are not high (e.g., near a separation point), this assumption does not hold and produces inaccurate results. If an appropriate model for the time derivative can be obtained for non-equilibrium flows, paired with the decoupled non-equilibrium model approach introduced by Hickel *et al.*, a wall model that includes the effects of the pressure gradient and convective terms can be constructed with a computa-

tional cost and complexity rivaling that of an equilibrium wall model while also providing accurate predictions in strong non-equilibrium flows.

1.4 Present Work

Following the developments above, the objective of the present work is to approximate the non-equilibrium (convective and pressure gradient terms) and time derivative through development of a low-cost ODE-based non-equilibrium wall model. This is accomplished by extending the work of Hickel *et al.* [18] using high-order polynomials to approximate the convection profile of the non-equilibrium terms. The approximation of the non-equilibrium terms is performed by a polynomial interpolation of the LES solution. Thus, it does not require an embedded resolved grid within the wall model region that is required by most non-equilibrium models. This significantly reduces the complexity of the implementation and memory requirements of the model. Additionally, because the solutions are decoupled (as enabled by the approximation of the non-equilibrium terms), the direct solution of the time derivative of the non-equilibrium wall model can be neglected and the effects of the temporal evolution of the flow are instead approximated using an empirically built lag model based on the degree of non-equilibrium of the flow. As a result, this model does not suffer from increased time step restrictions of traditional non-equilibrium wall models, which results in a computational cost several times less than that of traditional non-equilibrium wall models. The overall cost is similar to that of an equilibrium wall model. This set of approximations enables the first TBLE based non-equilibrium wall model that neglects solving the time derivative without producing an over-prediction in the wall shear stress for flows with strong non-equilibrium effects.

To assess this model compared to the current state-of-the-art approaches, wall resolved LES were run on two cases with strong non-equilibrium effects. The first is the NASA Wall Mounted Hump ($Re = 936,000, M = 0.1$). The second is an iced NACA 63A213 Airfoil ($Re = 250,000, M = 0.2$). Results from the first case were used to build an empirical lag

model that accounts for the absence of the time derivative. The wall model equations were then solved on coarser implementations of the instantaneous flow fields from both cases to provide details on the effects of the parameters of the wall models over a wider range of conditions. Results showed that a higher-order interpolation of the non-equilibrium terms did not yield notably more accurate predictions of the skin friction, but the choice of wall model eddy viscosity formulation did. Formulations of the eddy viscosity that account for the fact that the approximation of the convective terms resolves a portion of the unresolved shear stresses gave better predictions of the skin friction.

The proposed non-equilibrium wall model was implemented alongside the commonly used equilibrium wall model of Kawai & Larsson (which is comparable in terms of computational cost). In addition, WMLES using these two models with highly underresolved grids were run on both the wall mounted hump and the iced airfoil and compared to the wall resolved LES results of the same cases. The new non-equilibrum wall model was able to predict the separation at the trailing edge of the wall mounted hump with much better agreement to the wall resolved LES flow field. Additionally, a significantly better prediction of the skin friction coefficient was obtained with the non-equilibrium wall model. For the iced airfoil, both the separated flow region and the laminar flow region were better predicted by the non-equilibrium wall model in terms of the mean flow field and the skin friction coefficient. Slight improvements in the predicted pressure coefficient were also observed. Results showed strong indication that the proposed non-equilibrium wall model can offer better predictions of non-equilibrium flows with negligible computational cost increase compared to equilibrium wall models, many times less than that of a traditional non-equilibrium wall model.

CHAPTER 2

FORMULATION

2.1 Large Eddy Simulation

The compressible continuity and momentum equations for Large Eddy Simulation; e.g., as given by Vreman [30], are

$$\frac{\partial \overline{\rho}}{\partial t} + \frac{\partial \overline{\rho}\tilde{u}_i}{\partial x_i} = 0 \tag{2.1}$$

$$\frac{\partial \overline{\rho}\tilde{u}_i}{\partial t} + \frac{\partial \overline{\rho}\tilde{u}_i\tilde{u}_j}{\partial x_j} = -\frac{\partial \overline{P}}{\partial x_i} + \frac{\partial}{\partial x_j}(\overline{\sigma}_{ij} - \overline{\rho}\tau^r_{ij}) \tag{2.2}$$

where $\bar{(\cdot)}$ denotes the Reynolds-averaged filtering operation, $\tilde{(\cdot)}$ denotes the Favre-averaged filtering operation [31], σ_{ij} is the shear stress tensor, and τ_{ij} is the residual stress tensor, defined as

$$\tau_{ij} = u_i\tilde{u}_j - \tilde{u}_i\tilde{u}_j. \tag{2.3}$$

The residual stress tensor is calculated using the Smagorinsky-Lilly model [32], where

$$\tau_{ij} = -2(C_s\Delta)^2|\sqrt{2S_{ij}S_{ij}}|S_{ij} + \frac{1}{3}\tau_{kk}\delta_{ij}. \tag{2.4}$$

Here, Δ denotes filter width, taken as the cube root of the cell volume, and C_s denotes the Smagorinsky constant. The Smagorinsky constant is calculated using the dynamic model of Germano *et al.* [33].

2.2 Thin Boundary Layer Equations

Based on an order of magnitude analysis of the Navier-Stokes equations near the wall, the thin boundary layer equations (TBLE) can be written as

$$\frac{\partial u_i}{\partial t} + u_j \frac{\partial u_i}{\partial x_j} + \frac{1}{\rho}\frac{\partial P}{\partial x_i} = \frac{\partial}{\partial x_n}\left[(\nu + \nu_t)\frac{\partial u_i}{\partial x_n}\right] \tag{2.5}$$

where n denotes the wall normal direction, i denotes the wall parallel directions, and $j = 1, 2, 3$. In comparison to the Navier-Stokes equations, only the wall-normal diffusion term is retained. However, the unsimplified TBLE require the solution of derivatives in both wall parallel directions and time. Computationally, this poses a challenge in terms of both cost and complexity. Various simplifications can be made to the above equations, resulting in wall model formulations that retain or neglect the time derivative and/or wall parallel derivatives.

2.3 Equilibrium WMLES

For the equilibrium wall model (EQWM) approach introduced by Kawai & Larsson [2], the pressure gradient, convective, and time derivative terms are assumed to balance exactly, such that the left hand side of Eq. (2.5) reduces to zero. Additionally, the flow is assumed to remain in-plane and parallel to the wall throughout the wall model region. Without loss of generality, using a coordinate transform to wall parallel and wall normal coordinates and velocities, x, U and y, V, respectively, the governing EQWM equation can be written as

$$\frac{d}{dy}\left[(\mu + \mu_t)\frac{dU}{dy}\right] = 0, \qquad 0 \leq y \leq h_{wm}. \tag{2.6}$$

The no-slip boundary condition is applied at the wall and the LES velocity is applied at the wall model height, h_{wm}; i.e.,

$$U(0) = 0, \qquad U(h_{wm}) = U_{LES}\Big|_{h_{wm}} \tag{2.7}$$

The wall model eddy viscosity μ_t is given by a mixing length formula with Van Driest near wall damping such that

$$\mu_t = \mu\kappa\rho y^+\mathcal{D}, \qquad \mathcal{D} = [1 - \exp(-y^+/A^+)^2]. \tag{2.8}$$

Here, the damping constant A^+ is generally taken as 17. Integrating Eq. (2.6) shows that the shear stress is constant within the wall model, which is the so-called "stress balance" model. In the limit of vanishing viscosity (i.e. high Reynolds number), the velocity profile given by Eq. (2.6) reduces to the instantaneous log-law model. This wall model does not require the evaluation of derivatives in time or the wall parallel direction. Thus, it can be solved numerically at a low computational cost and complexity, generally by iteratively solving the governing equations until convergence. Since the solution depends only on the LES velocity at the wall model height and does not need to be retained after the wall shear stress is calculated, it has very low memory requirements and is straightforward to program on modern parallel computer architectures.

2.4 Unsteady Non-Equilibrium WMLES

For non-equilibrium wall models (NEQWM), the wall parallel TBLE are solved exactly, including wall parallel derivatives and time derivative, without assumptions on the direction of the flow within the wall model region ($0 \leq y \leq h_{wm}$). This results in the following coupled set of wall parallel momentum equations:

$$\frac{\partial U}{\partial t} = -U\frac{\partial U}{\partial x} - V\frac{\partial U}{\partial y} - W\frac{\partial U}{\partial z} - \frac{1}{\rho}\frac{\partial P}{\partial x} + \frac{d}{dy}\Big[(\nu + \nu_t)\frac{dU}{dy}\Big], \tag{2.9}$$

$$\frac{\partial W}{\partial t} = -U\frac{\partial W}{\partial x} - V\frac{\partial W}{\partial y} - W\frac{\partial W}{\partial z} - \frac{1}{\rho}\frac{\partial P}{\partial z} + \frac{d}{dy}\Big[(\nu + \nu_t)\frac{dW}{dy}\Big]. \tag{2.10}$$

These equations are evolved in time with the boundary condition at the wall model height updated by the LES solver at each time step. To evaluate the wall parallel gradients, an embedded grid within the LES solver is required. This grid is typically designed with approximately 30-100 wall normal grid points, which poses significant challenges for calculations that involve complex geometries. Additionally, by solving the unsteady form of the TBLE, the CFL constraints for the LES solver are generally dictated by the CFL constraint of the wall model grid since the grid spacing within the wall model can be orders of magnitude smaller than the wall model height. This significantly increases the overall computational cost compared to equilibrium wall models due to the decreased time step of the LES solver. In addition, no savings in computational cost can be obtained by using the steady form of the TBLE with wall parallel gradients since it would require the solution of a nonlinear boundary value problem whose domain spans the entire near wall region. This instead creates a significantly more difficult problem.

To reduce the complexity of an embedded grid within the LES solver, Hickel *et al.* proposed an approximate form of the pressure and gradient terms. The pressure gradient was assumed constant in the wall model region, dictated by the pressure gradient of the LES solver at the wall model height. The convective term was then modeled as zero at the wall and matching the negative of the pressure gradient at the wall model height solving the following equations

$$\frac{\partial U}{\partial t} = -(1 - \frac{y}{h_{wm}})\frac{1}{\rho}\frac{\partial P}{\partial x}\Big|_{LES} + \frac{d}{dy}\Big[(\nu + \nu_t)\frac{dU}{dy}\Big], \tag{2.11}$$

$$\frac{\partial W}{\partial t} = -(1 - \frac{y}{h_{wm}})\frac{1}{\rho}\frac{\partial P}{\partial z}\Big|_{LES} + \frac{d}{dy}\Big[(\nu + \nu_t)\frac{dW}{dy}\Big]. \tag{2.12}$$

This formulation requires only derivatives in the wall normal direction and time, which significantly reduces the complexity of the wall model. However, the computational cost is still significantly higher than an equilibrium wall model due to the CFL restrictions of the time derivative. Additionally, the errors introduced by assuming that the convective term matches the pressure gradient term outside the viscous sublayer can be significant since this assumption does not necessarily hold for non-equilibrium flows. This assumption is also ill-posed if the wall model height is not within the log-layer, which can easily occur when simulations are performed on flows without a priori knowledge of the flow field.

2.5 Steady Non-Equilibrium WMLES

In the proposed non-equilibrium wall model approach, an approximate form of the wall parallel TBLE is solved. Likewise to the equilibrium wall model, the flow is assumed to be parallel and in-plane, such that the TBLE can be reduced to a single equation for the wall parallel momentum with the appropriate coordinate transform. The governing equation for this model does not directly include the time derivative, convective, and pressure gradient terms, but instead includes a forcing term to approximate the effect of these; i.e.,

$$\frac{d}{dy}\left[(\nu+\nu_t)\frac{dU}{dy}\right] = F(y), \qquad 0 \leq y \leq h_{wm}, \tag{2.13}$$

where

$$F(y) \approx U\frac{\partial U}{\partial x} + V\frac{\partial U}{\partial y} + \frac{1}{\rho}\frac{\partial P}{\partial x}. \tag{2.14}$$

The treatment of the time derivative is described in Section 2.5.2.

The forcing term in Eq. (2.13) is approximated to spatially decouple the wall model equations and eliminate the need to evaluate wall parallel derivatives. The following characteristics are desired for a suitable approximation of $F(y)$:

- It should include the effects of both the pressure gradient and convective terms.
- It should not require matching of the pressure gradient and convective terms in any particular region.
- At the wall model height, the forcing term of the wall model should match the convective and pressure gradient terms of the LES solver.
- At the wall, the forcing term of the wall model should match the pressure gradient of the LES solver.

Since the wall model interface location is generally several grid points above the wall (e.g., for reasons outlined by Larsson *et al.* [3]), an appropriate method of modeling the forcing term that meets the desired characteristics is by interpolating the corresponding LES values at these grid points. This is accomplished using an n-th order polynomial interpolation of the pressure gradient and convective terms given by the LES solution at the wall normal LES grid points that fall within the wall model layer. The stencil used has the form

$$F(y) = \sum_{i=0}^{n} c_i y^i \approx U\frac{\partial U}{\partial x} + V\frac{\partial U}{\partial y} + \frac{1}{\rho}\frac{\partial P}{\partial x}. \tag{2.15}$$

Reasonable values of n range from 1 to 4. The lower bound is given under the reasoning that no additional work is required for a first-order approximation compared to no approximation since the gradients are already evaluated by the LES solver at the wall and the wall model interface point. The upper bound is given under the reasoning that the wall model height is taken at generally 3 to 5 grid points away from the wall.

In this work, the effects of the interpolation order on the accuracy of the shear stress prediction is explored to see if benefits over the linear profile of Hickel *et al.* can be gained. A first order approximation is then implemented, such that within the wall model layer, the forcing approximation matches the LES pressure gradient at the wall and linearly increases/decreases to the sum of the LES pressure gradient and convective terms at the

wall model height, correcting the unnecessary assumption by Hickel *et al.* that the pressure gradient and convective term balance at the wall model height. For further generality, the approximation does not assume that the pressure gradient is constant within the wall model layer, but instead relies on the evaluation of the sum of both the pressure gradient and convective terms.

2.5.1 Eddy Viscosity

Since a portion of the subgrid-scale shear stresses are resolved by the approximation of the convective terms, the eddy viscosity must be modified to account for this effect [1]. Several works in wall modeling have formulated eddy viscosity models with the effects of the pressure gradient included. However, as stated by Larsson *et al.* [3], including the pressure gradient while neglecting the convective term is physically inconsistent, and as such, models that include only the pressure gradient must be modified. In the proposed NEQWM approach, the wall model eddy viscosity is calculated using the formulation by Duprat *et al.* [34], but with modifications to include the effects of the convective terms and the variation of these terms within the wall model layer since the original formulation only included the pressure gradient. A forcing velocity, u_f, analogous to the pressure velocity, u_p, by Simpson [35], is defined as

$$u_f(y) = \left| \frac{\mu}{\rho} F(y) \right|^{\frac{1}{3}}. \tag{2.16}$$

A modified inner velocity scale $u_{f\tau}$ can then be defined as the vector sum of the forcing velocity and the friction velocity u_τ; i.e.,

$$u_{f\tau}(y) = \sqrt{u_f^2(y) + u_\tau^2}. \tag{2.17}$$

Given the modified inner velocity scale, the nondimensional velocity U^* and wall distance y^* are defined as

$$U^* = \frac{U}{u_{f\tau}|_{y=0}}, \qquad y^* = \frac{y u_{f\tau}|_{y=0}}{\nu}, \tag{2.18}$$

which remain well defined at the point of flow separation in contrast to the traditional nondimensional velocity u^+ and wall distance y^+. Note that this scaling is consistent with the formulation by Manhart [36] since at the wall the no-slip condition reduces the forcing velocity to the pressure velocity. Furthermore, a nondimensional parameter α can be defined as

$$\alpha(y) = \frac{u_\tau^2}{u_{f\tau}^2} = \frac{u_\tau^2}{u_f^2 + u_\tau^2} \in [0, 1], \tag{2.19}$$

which quantifies the degree of equilibrium that the flow is in. A value of $\alpha = 1$ corresponds to a zero pressure gradient and convection-free flow. A value of $\alpha = 0$ corresponds to a separation point. The modified Duprat eddy viscosity is then defined as

$$\nu_t = \nu\kappa y^*[\alpha + y^*(1-\alpha)^{\frac{3}{2}}]^{0.78}(1 - e^{\frac{-y^*}{1+17\alpha^3}})^2. \tag{2.20}$$

2.5.2 Time Derivative

Spatially decoupling the convective terms in the non-equilibrium wall model equations by approximating them instead of direct evaluation provides an opportunity for dramatically lowering the computational cost of the model. In addition, neglecting the time derivative reduces the governing equation to a set of decoupled nonlinear boundary value problems in one dimension, similar to the equilibrium wall model equations. Prior to the forcing term approximation, the steady form of the non-equilibrium equations is considerably more expensive to solve than the unsteady form since the coupling caused by the wall parallel gradients requires the solution of a single nonlinear three dimensional boundary value problem over the entire near wall region. By neglecting the time derivative, the wall model solution is not subject to CFL constraints, and the time step of the LES solver is not limited by

the wall model grid, which is the case for traditional non-equilibrium wall models. Therefore, the computational cost and memory requirements of solving this non-equilibrium wall model are essentially identical to solving an equilibrium wall model, which can be over an order of magnitude less than a time-dependent non-equilibrium wall model while still resolving the non-equilibrium effects.

Despite the potential benefits, there are also several potential limitations that must be considered. By neglecting the time derivative, the governing NEQWM equation becomes a boundary value problem (BVP) with time-dependent boundary conditions. In contrast, the physics dictate that the flow should be treated as an initial value problem (IVP) with time-dependent boundary conditions since maintaining the convective term but neglecting the time derivative violates the fact that fluid accelerations are Lagrangian in nature [3]. Attempts to model the time derivative in the wall model region are very sparse in the literature, owing to the fact that neglecting the term dramatically increases the computational cost of traditional time-dependent non-equilibrium wall models while introducing additional errors. Some insight can be gained from early works in wall modeling since analytic wall model formulations neglect the time derivative. Hoffmann and Benocci [11] showed that the effect of the time derivative was to increase the wall shear stress with decreasing velocity and vice versa. They attempted to model the time derivative as a source term in a BVP solution by scaling the wall model velocity by the time derivative of the velocity of the LES solution at the wall model height using the relation

$$\frac{\partial U(y)^n}{\partial t} \approx \frac{\partial u^n_{LES}}{\partial t} \frac{U(y)^n}{u^n_{LES}}. \tag{2.21}$$

Here, $U(y)$ denotes the wall model velocity, u_{LES} denotes the velocity of the LES solution at the wall model height, and the subscript n denotes the current time step. This approximation worked well for attached flows, but performed poorly for flows where the velocity gradients at the wall were not high such as near separation points. For the latter class of

flows, no suitable approximation has been found to treat the time derivative because of their highly unsteady nature. The general consensus in the wall modeling community is that the non-equilibrium wall model equations must be solved as a time-stepping problem, both for physical consistency and due to their simplicity in solving for traditional non-equilibrium wall modeling approaches [3]. Non-equilibrium wall models that retain terms such as the pressure gradient but neglect the time derivative show overpredictions in the wall shear stress [29]. This can be attributed to the compounding nature of the wall shear stress error. Overpredictions in the wall shear stress cause higher velocity gradients near the wall, which increase the magnitude of the convective term and subsequently causes higher predictions of the wall shear stress. This effect is less severe for underpredictions since for a zero convective term magnitude a finite wall shear stress is still obtained.

To obtain a significant increase in time step by treating the problem as steady instead of unsteady, a suitable model for the time derivative that is valid for non-equilibrium flows must be derived. In this work, a novel way of treating the time derivative is proposed. Instead of modeling the effect of the time derivative on the solution of the wall model equations, and thus the wall shear stress as attempted by Hoffmann and Benocci, the effect of the time derivative on the *changes* in the wall shear stress between time steps is modeled. As a result, the proposed non-equilibrium model does not require the solution of a time stepping problem but still resolves the effects of the unsteady term on the wall shear stress even in separated flows. This is accomplished while retaining the computational benefits of solving a one dimensional BVP. The physical basis of this model comes from the difference in the solutions of IVP and BVP problems, as highlighted in the following example.

Example Diffusion Problem

For a BVP, changes in the boundary conditions propagate throughout the entire solution at infinite speed, whereas for an IVP the changes propagate at a finite speed. Thus, the IVP solution "lags" behind the BVP solution. As a result, a BVP-based wall model over-

predicts the changes in the wall shear stress in comparison to an IVP-based wall model. This corroborates the findings of Hoffmann and Benocci, which show the effect of the time derivative is to increase the wall shear stress with decreasing velocity and vice versa. This error must be accounted for, and the forcing term has an effect on this error.

The differences in the IVP and BVP solutions can be illustrated in the following example. Consider diffusion with a forcing term, F, and time-dependent boundary conditions similar to the wall model equations; i.e.,

$$\text{IVP} : \frac{\partial u}{\partial t} = \alpha \frac{\partial^2 u}{\partial x^2} - F, \tag{2.22}$$

and

$$\text{BVP} : \alpha \frac{\partial^2 u}{\partial x^2} = F. \tag{2.23}$$

The boundary conditions are also specified similarly to the wall model equations; i.e., zero at the wall and matching some function $g(t)$ at a height h:

$$u(0,t) = 0, \qquad u(h,t) = g(t). \tag{2.24}$$

For a given value of $g(t)$, the steady-state solution of the IVP (u_{IVP}) is equivalent to the solution of the BVP (u_{BVP}). However, if not given enough time to attain steady-state, u_{IVP} lags behind u_{BVP} as it retains some information from its previous state. The amount of lag can be quantified by the ratio of the time derivatives of the boundary condition ($\partial g/\partial t$) and the solution ($\partial u/\partial t$). If the IVP solution advances much faster than the boundary condition changes (i.e. $|\partial u/\partial t| >> |\partial g/\partial t|$), then the IVP solution has sufficiently attained steady-state and the BVP approximation should be valid. If the IVP solution does not advance much faster than the boundary condition changes, then the IVP solution has not sufficiently attained steady-state but instead lies in between the solution at the previous time step and the BVP solution at the current time step.

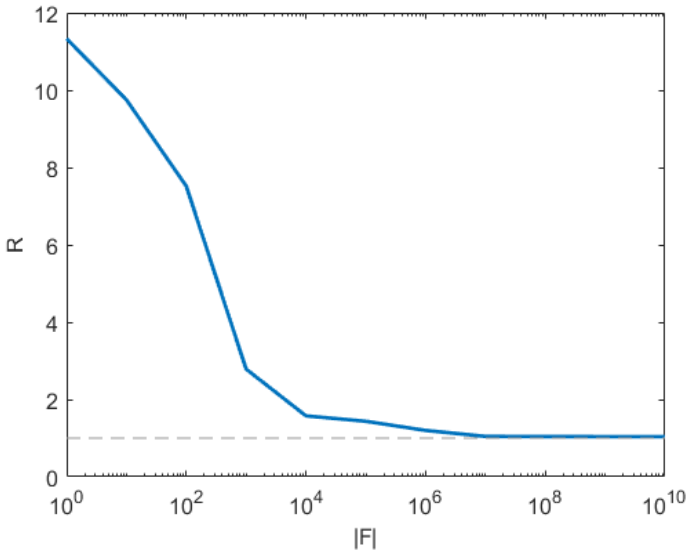

Figure 2.1: BVP approximation error with respect to the forcing term magnitude.

Since the $\partial u/\partial t$ term contains F, the forcing term can be used to quantify the lag between the IVP and BVP solutions. For large values of $|F|$, the steady-state assumption holds and the BVP solution can be used, whereas for small $|F|$, steady-state is not attained. As previously mentioned, the unsteady solution to the IVP at the current time step lies somewhere between the solution of the previous time step and the steady state solution. Therefore, the IVP solution at the current time step can instead be approximated as some combination of the BVP solution at the current time step and the solution at the previous time step. Let the ratio R be defined as

$$R = \frac{\tau^n_{0(BVP)} - \tau^{n-1}_{0(IVP)}}{\tau^n_{0(IVP)} - \tau^{n-1}_{0(IVP)}} \tag{2.25}$$

where τ_0 denotes the gradient at the wall of the IVP and BVP solutions, respectively, and the superscripts n and $n-1$ denote the current and previous time steps. The ratio R shows the error of the BVP approximation for predicting the temporal evolution of the IVP solution. As the forcing term becomes large, R converges to unity indicating that the BVP approximation is valid for large F. The changes are overpredicted for small values of F, as shown in Figure 2.1.

The desired property of the proposed wall model is to predict the unsteady evolution of the wall shear stress as a function of steady state solutions. Thus, the overprediction must be accounted for. This is achieved by blending the previous solution and the current steady state solution. A reduction factor, ζ, is introduced as some function of the forcing term F,

$$\zeta = h(F) \in [0, 1], \tag{2.26}$$

such that

$$\lim_{F \to \infty} \zeta = 1. \tag{2.27}$$

Assuming that the gradient at the wall at the previous time step was approximated correctly, the gradient at the current time is approximated as a blending of the previous gradient and the current BVP gradient,

$$\tau_0^n = (1 - \zeta)\tau_0^{n-1} + \zeta \tau_{0(BVP)}^n \approx \tau_{0(IVP)}^n. \tag{2.28}$$

The desired behavior of ζ is such that as the forcing term gets larger, the predicted wall shear stress tends toward the steady state solution, and vice versa. This reduction factor is the basis for the proposed BVP-based NEQWM, which neglects the time derivative but corrects for the overpredictions in the wall shear stress.

2.5.3 Reduction Factor

Since the desired behavior of the reduction factor is for it to tend towards zero or one as the flow tends towards equilibrium or non-equilibrium, the reduction factor must be a function of some quantitative representation of the non-equilibrium of the flow. A suitable representation of this is the term $\overline{\beta}$, which is defined as the complement of the average

value of α across the wall model layer and given by

$$\overline{\beta} = 1 - \overline{\alpha} = \frac{(\overline{u_f})^2}{(\overline{u_{f\tau}})^2} = \frac{(\overline{u_f})^2}{(\overline{u_f})^2 + u_\tau^2}. \tag{2.29}$$

For regions of the flow dominated by non-equilibrium effects, $\overline{\beta}$ approaches one, whereas $\overline{\beta}$ approaches zero in equilibrium regions. The ideal reduction factor is assumed to be $\overline{\beta}$ raised to some empirically determined coefficient c_1,

$$\zeta = \overline{\beta}^{\,c_1}. \tag{2.30}$$

The wall shear stress τ_w at a given wall grid point is then given as

$$\tau_w^n = (1 - \zeta)\tau_w^{n-1} + \zeta\tau_{w(wm)}^n, \tag{2.31}$$

where n and $n - 1$ denotes the current and previous time step and $\tau_{w(wm)}$ denotes the solution of Eq. (2.13), the steady state non-equilibrium wall model equation.

CHAPTER 3
METHODOLOGY

3.1 Geometry and Flow Conditions

Two cases were chosen for the optimization and validation of the NEQWM. The first case, the NASA wall mounted hump, was used to find the optimal parameters for the NEQWM, while the second case, an iced NACA 63A213 airfoil, was used to validate the empirically built NEQWM against a distinctly different flow. The former is a high Reynolds number flow with turbulent separation, whereas the latter is a flow with laminar separation and transition at a moderate Reynolds number.

3.1.1 Wall Mounted Hump

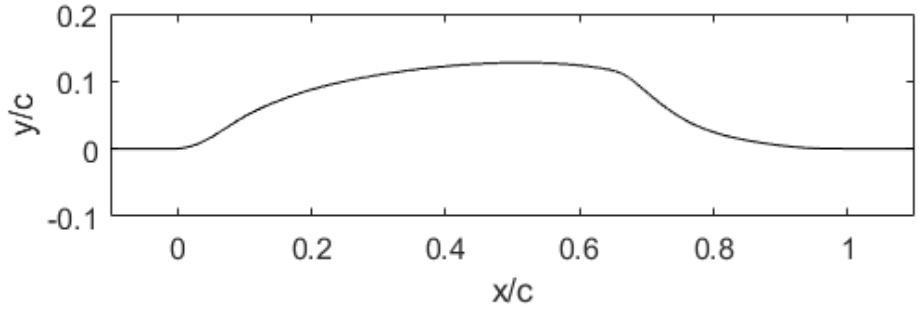

Figure 3.1: NASA wall mounted hump geometry.

The NASA wall mounted hump consists of a smooth extruded hump profile within a wind tunnel, as shown in Figure 3.1, operating at a Reynolds number of 936,000 and a Mach number of 0.1 [37]. Since the flow contains strong favorable and adverse pressure gradients, as well as separation and reattachment, it serves as a suitable test case for the NEQWM. An inlet profile is used with a boundary layer thickness of $\delta = 8.3\%$ of the hump chord. The inlet profile is specified at $x/c = -2.14$ using a $1/7$th power law boundary layer

with hyperbolic tangent blending to smooth the slope discontinuity at the boundary layer height; i.e.,

$$u_{in}(y) = \left(\frac{y}{\delta}\right)^{\frac{1}{7}}(1-\psi)+\psi, \qquad \psi = \frac{1}{2}tanh(25(y-\delta)+1). \tag{3.1}$$

3.1.2 Iced Airfoil

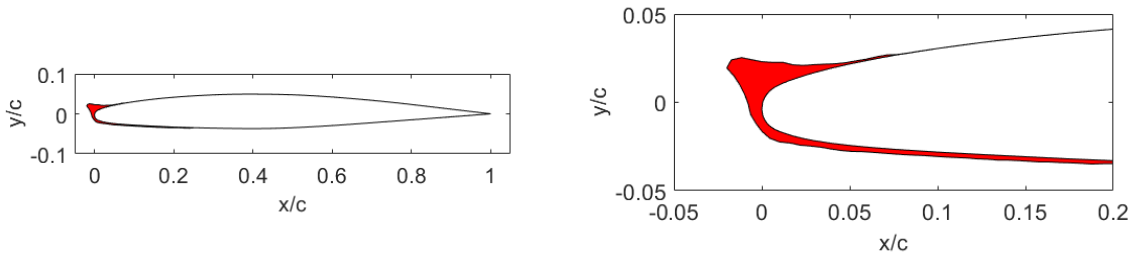

Figure 3.2: NACA 63A213 geometry with horn-shaped ice protrusion (red).

The second geometry is a NACA 63A213 airfoil with a "horn-shaped" ice profile protruding from the leading edge, as shown in Figure 3.2. The ice profile is generated using a reduced-order Proper Orthogonal Decomposition (POD) mode reconstruction [38]. The angle of attack is 9° to create separation at the iced leading edge and subsequent stall. A Reynolds number of 250,000 was chosen to include both laminar and turbulent flow regimes, and a freestream Mach number of 0.2 was chosen to minimize the effects of temperature boundary conditions on the flow.

3.2 Computational Approach

3.2.1 Solvers

Because of the large computational cost of performing wall-resolved simulations, WRLES were performed using PyFR, a GPU-accelerated higher-order flux reconstruction solver [39]. However, since the implementation of wall models is ill suited for higher-order solvers, WMLES were performed using RAPTOR, an in-house, staggered-grid, finite-volume solver.

A comparison of the two solvers are shown in the following subsections. For both solvers, the compressible Navier-Stokes equations were solved for 10 nondimensional time units, corresponding to 10 flows over chord. Solving was performed on the Hydra cluster at the Partnership for an Advanced Computing Environment (PACE) at Georgia Institute of Technology. RAPTOR was run on 625 cores with an estimated peak computing power of 1.75 TFLOPs while PyFR was run on 16 nVidia V100 GPUs with an estimated peak computing power of 76 TFLOPs.

WRLES/PyFR

A fourth-order discontinuous Galerkin method with flux reconstruction was utilized with the Roe-FDS and LDG schemes [40, 41]. A wall resolved implicit LES approach was used with no turbulence modeling, and an explicit four-stage Runge-Kutta method was used for time stepping. Anti-aliasing by means of the L_2 projection of the divergence flux with a quadrature degree of 9 was used for stabilizing.

WMLES/RAPTOR

The dynamic Smagorinsky LES approach was used with dual-time stepping utilizing a four-stage Runge-Kutta method. The wall model equations were solved by iteratively solving the tridiagonal system of equations using 40 unevenly spaced points until 9 orders of magnitude of residual reduction in the wall shear stress was observed.

RAPTOR-PyFR Validation

Wall-resolved LES were run using RAPTOR and PyFR on the wall mounted hump at a Reynolds number of 60,000 and Mach number of 0.2. The time-averaged streamwise velocity fields computed by RAPTOR and PyFR are shown in Figure 3.3 and 3.4, respectively, showing relatively good agreement between the two solvers. Good agreement in the time-averaged streamwise skin friction coefficient was also observed, but some peaks were

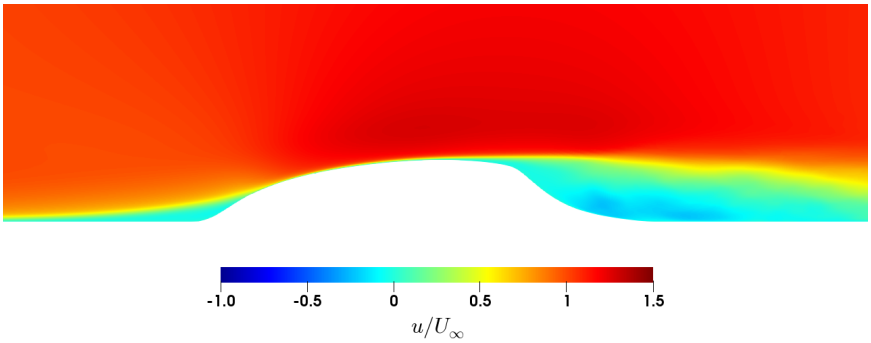

Figure 3.3: Time-averaged streamwise velocity contours for low Reynolds number wall mounted hump solved by RAPTOR.

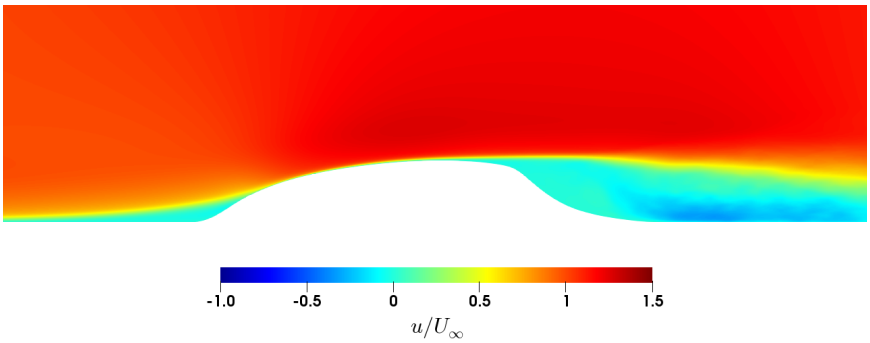

Figure 3.4: Time-averaged streamwise velocity contours for low Reynolds number wall mounted hump solved by PyFR.

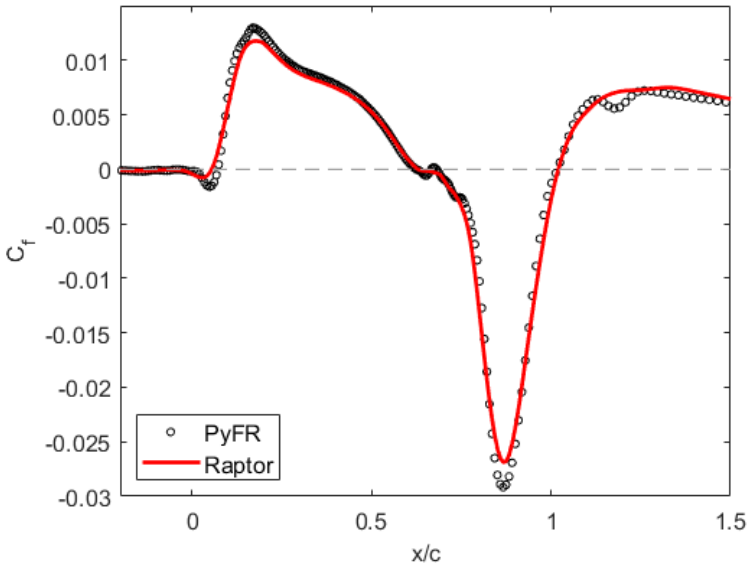

Figure 3.5: Time-averaged streamwise skin friction coefficient for the low Reynolds number wall mounted hump.

overpredicted in magnitude by PyFR in comparison to RAPTOR, as shown in Figure 3.5. The solvers also showed excellent agreement in the predicted pressure coefficient prior to the separation point with some underprediction by PyFR in comparison to RAPTOR aft of the separation point, as shown in Figure 3.6.

3.2.2 Meshes

For both the wall mounted hump and the iced airfoil, two dimensional meshes were generated and extruded to create three dimensional periodic meshes. Between the WRLES and WMLES approaches, the wall parallel grid spacing was kept constant while the wall normal grid spacing was varied. The number of grid points (N) and grid spacing at the surface (Δ^+) are shown in Table 3.1 and Table 3.2, with the scripts x, y, and z denoting the chordwise, wall normal, and spanwise directions, respectively. The grid spacing is nondimensionalized by the viscous length scale of a flat plate with identical length and flow conditions. The wall model height h^+_{wm} was taken at the 4th grid point normal to the surface.

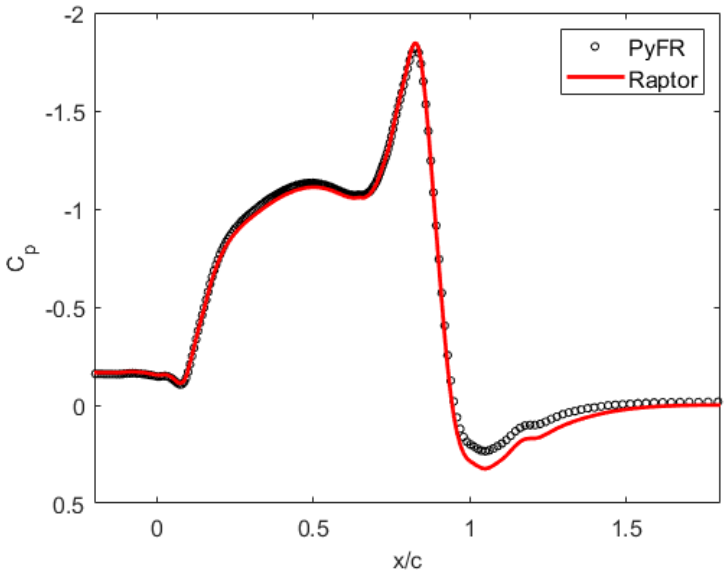

Figure 3.6: Time-averaged pressure coefficient for the low Reynolds number wall mounted hump.

Wall Mounted Hump

A highly-orthogonal mesh was generated by extruding the hump profile in the normal direction. For the WMLES approaches, the entire mesh was structured, whereas for the WRLES approach, an unstructured mesh was used after extruding the hump profile for 20% of the chord. Velocity inlet and pressure outlet boundary conditions were used, and an adiabatic, slip boundary condition was applied to the top surface of the wind tunnel. For the hump surface, an adiabatic boundary condition was specified. The extent of the spanwise direction was 1.2% of the chord.

Table 3.1: Grid metrics for wall resolved and wall modeled approaches for the wall mounted hump.

Method	N_x	N_y	N_z	N_{total}	Δx^+_{min}	Δy^+	Δz^+	h^+_{wm}
WRLES	1250	200	20	$5 \cdot 10^6$	30	1	30	140
WMLES	1250	100	20	$2.5 \cdot 10^6$	30	30	30	140

Iced Airfoil

O-type grids were generated for both the wall modeled and wall resolved approaches by extruding the airfoil profile normal to the surface for 50 chord lengths. The airfoil surface was given an adiabatic boundary condition while the farfield was given a characteristic Riemann invariant boundary condition. The extent of the spanwise direction was 15% of the chord.

Table 3.2: Grid metrics for wall resolved and wall modeled approaches for the iced airfoil.

Method	N_x	N_y	N_z	N_{total}	Δx^+_{min}	Δy^+	Δz^+	h^+_{wm}
WRLES	1024	128	50	$6.55 \cdot 10^6$	30	1	30	160
WMLES	1024	64	50	$3.28 \cdot 10^6$	30	30	30	160

3.3 Wall Model Verification and Parameter Optimization

Initial verification and comparison of the wall modeled approaches was performed by interpolating instantaneous WRLES flow fields to the coarser wall model grid and solving the wall model equations to find the next instantaneous wall shear stress distribution. This calculated wall shear stress was then compared to the WRLES shear stress. Parameter optimization for the NEQWM was performed by minimizing the L_2 norm of the wall shear stress error using a gradient descent method across 100 instantaneous flow fields and wall model heights (h^*_{wm}) of 30, 50, and 120. The optimal parameters were determined from only the wall mounted hump flow fields, and these parameters were then used for simulating the iced airfoil to determine if the empirical parameters were suitable for highly dissimilar flows.

3.4 Post-Processing

After 5 time units of the wall mounted hump, and 2 time units of the iced airfoil, the flow was assumed to be fully developed. Statistical quantities were then acquired and analyzed

until 10 time units with 200 instantaneous flow fields acquired per flow over chord. Averaging was performed over time and along the spanwise direction. For simulations performed using the discontinuous Galerkin method, a centered reconstruction was performed along coincident solution points prior to spanwise averaging. Comparison between the wall-resolved and wall-modeled approaches was performed with respect to the mean flow field, skin friction coefficient, pressure coefficient, and velocity profiles.

CHAPTER 4

RESULTS

4.1 Wall Model Optimization

4.1.1 Optimal Coefficients

By interpolating the instantaneous wall resolved LES flow fields for the wall mounted hump onto a coarser grid, the wall model equations were solved to assess the ability of the model to predict the evolution of the skin friction coefficient between time steps in comparison to the wall resolved results. The optimal coefficient c_1 for the reduction factor ζ was determined to be

$$c_1 = 0.331 \tag{4.1}$$

by minimizing the L_2 norm of the skin friction prediction error in the interpolated wall model approach. This coefficient also gave accurate predictions of the wall shear stress for the iced airfoil without a priori knowledge of the flow. For separated turbulent flow regimes, the reduction factor generally attained a value between 0.6 and 0.8 due to the presence of strong non-equilibrium effects, whereas the reduction factor was lower in laminar flow regimes (0.4 - 0.6) as the non-equilibrium effects were significantly reduced.

4.1.2 Forcing, Eddy Viscosity, and Reduction Factor Effects

The effects of the forcing term, wall model eddy viscosity choice, and reduction factor, were independently explored using the interpolated wall model approach. Using an instantaneous iced airfoil flow field interpolated on a coarser grid, the wall model equations were solved with varying parameters and models to determine their impact on the predicted changes in the wall shear stress. The various models are denoted by the following labels:

- **EQ**: Kawai-Larsson EQWM.
- **NEQ-P1-ML**: NEQWM with 1st order forcing approximation and mixing length eddy viscosity.
- **NEQ-P1-DU**: NEQWM with 1st order forcing approximation and Duprat eddy viscosity.
- **NEQ-P1-DU-RF**: NEQWM with 1st order forcing approximation, Duprat eddy viscosity and reduction factor.

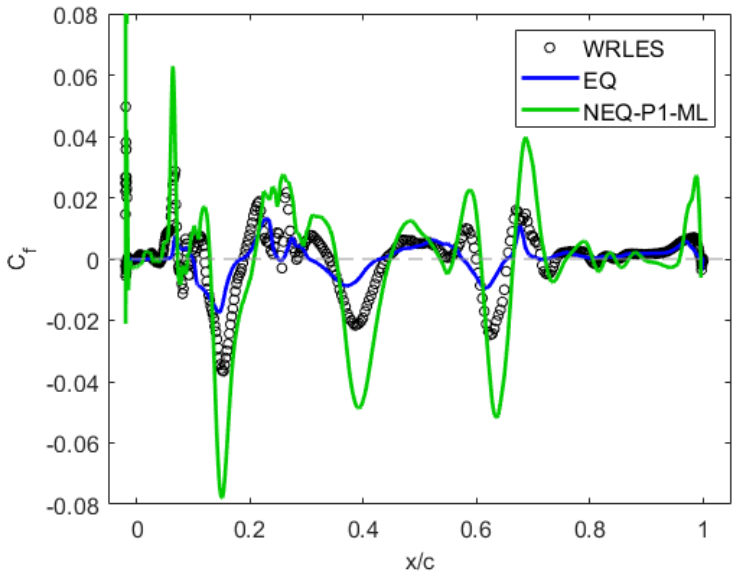

Figure 4.1: Predicted skin friction coefficient using the interpolated wall model approach with and without the forcing term.

A comparison of the instantaneous streamwise skin friction coefficient using the EQ and NEQ-P1-ML wall models is shown in Figure 4.1. With the inclusion of the forcing term, the general shape of the skin friction profile was much better predicted in comparison to the EQWM. Since the EQWM solution is monotonic and does not allow for inflections in the velocity profile, the direction of the predicted skin friction coefficient follows the direction of the LES velocity at the wall model height. This is not necessarily true in non-equilibrium flows, as seen at $x/c = 0.35$ and 0.58. These inflections were better captured

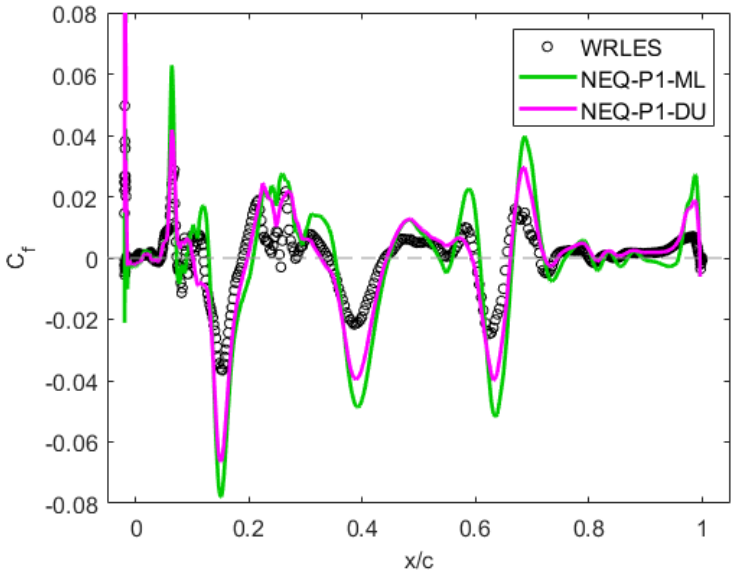

Figure 4.2: Predicted skin friction coefficient using the interpolated wall model approach with the mixing length and Duprat eddy viscosities.

through use of the forcing term in the NEQ-P1-ML model, but the magnitude of the skin friction was significantly overpredicted since the temporal evolution was not accounted for.

The effects of changing the wall model eddy viscosity are shown in the comparison of the NEQ-P1-ML and NEQ-P1-DU models in Figure 4.2. The magnitude of the skin friction was generally decreased when using the Duprat eddy viscosity and in closer agreement with the WRLES skin friction, but the magnitude was still overpredicted since the temporal evolution had been neglected. Additionally, the shape of the skin friction profile was better predicted with the Duprat eddy viscosity, as evident near the trailing edge of the airfoil.

The results of including the reduction factor between time steps are shown in Figure 4.3 with the comparison of the NEQ-P1-DU and NEQ-P1-DU-RF models. The original EQ model is included as reference. With the reduction factor, the magnitude of the skin friction was predicted in excellent agreement with the WRLES results along the peaks and troughs. However, the skin friction was poorly predicted by all models in regions with strongly fluctuating skin friction, such as $x/c = 0.1$ and 0.3, as a result of the inability of the model to resolve small scale spatial and temporal fluctuations.

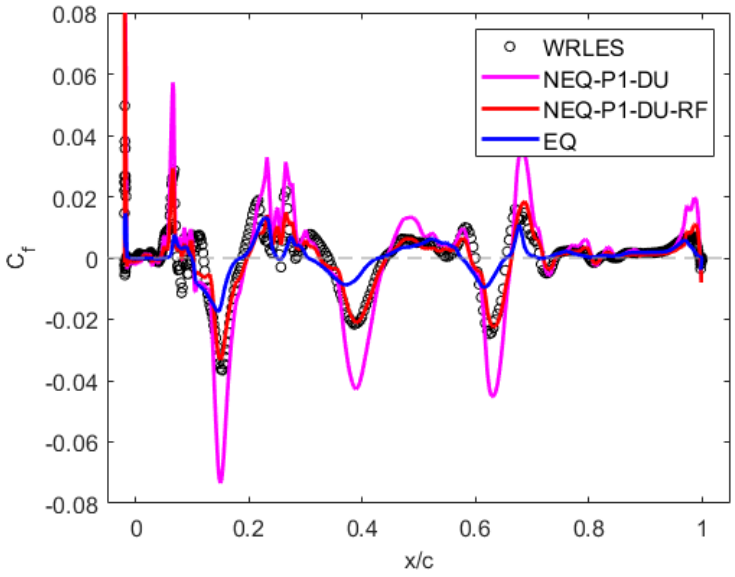

Figure 4.3: Predicted skin friction coefficient using the interpolated wall model approach with and without the reduction factor.

4.1.3 Forcing Approximation Order

The effect of the order of the polynomial approximation for the forcing term on the accuracy of the skin friction prediction is shown in Figure 4.4. First, second, and third order polynomial approximations were used, denoted by $P1$, $P2$, and $P3$, respectively, from the interpolation of evenly spaced grid points within the wall model region. Increasing the polynomial approximation order was observed to have very little impact on the predicted skin friction, and a higher polynomial approximation order did not necessarily result in a more accurate prediction. This effect can be attributed to two causes. First, the pressure gradient can be effectively approximated as constant within the wall model layer, thus the higher order approximations did not yield notably more accurate predictions of the pressure gradient. Second, although the convective term profiles resemble higher-order polynomials, they were damped near the wall due to the no-slip condition and their effect on the forcing term was negligible compared to the pressure gradient near the wall. As the wall normal distance increased, the convective term made a larger contribution to the forcing term, but the presence of small scale fluctuations in the convective term was notably less

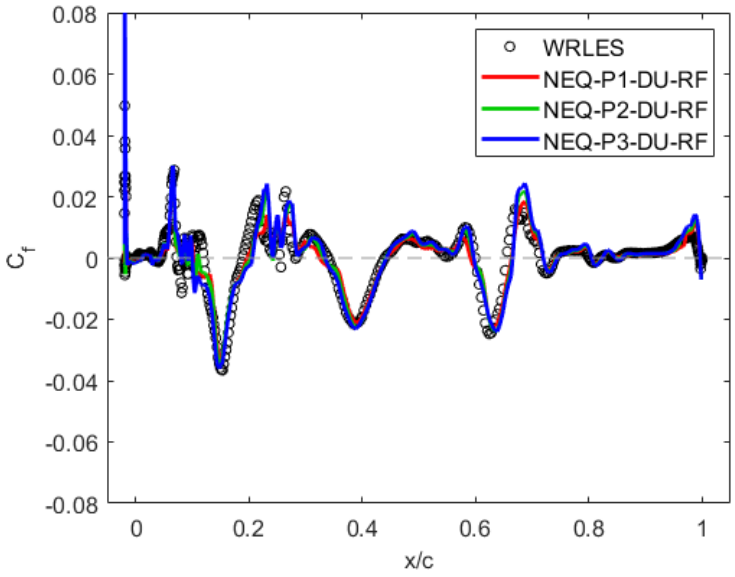

Figure 4.4: Predicted skin friction coefficient using the interpolated wall model approach for first, second, and third order polynomial approximations for the forcing term.

than near the wall. As such, a linear approximation could effectively model most of the contribution of the convective terms to the skin friction prediction.

Since the calculation of a higher-order forcing approximation is significantly more complex for certain solvers (e.g., unstructured solvers) and does not provide observable benefits, the forcing approximation was limited to a linear profile.

4.2 Wall Mounted Hump

The time-averaged streamwise velocity field from the WRLES, EQWMLES, and NEQWMLES approaches is shown in Figure 4.5. The WRLES flow field showed evident separation at the trailing edge of the hump and a region of strongly reversed flow aft of the hump. In comparison, the EQWMLES flow field showed only slight indication of separation at the trailing edge without any recirculation region. The NEQWM predicted the trailing edge separation significantly better than the EQWM, and an evident recirculation region was observed aft of the hump. However, the degree of the reversed flow and the length of the

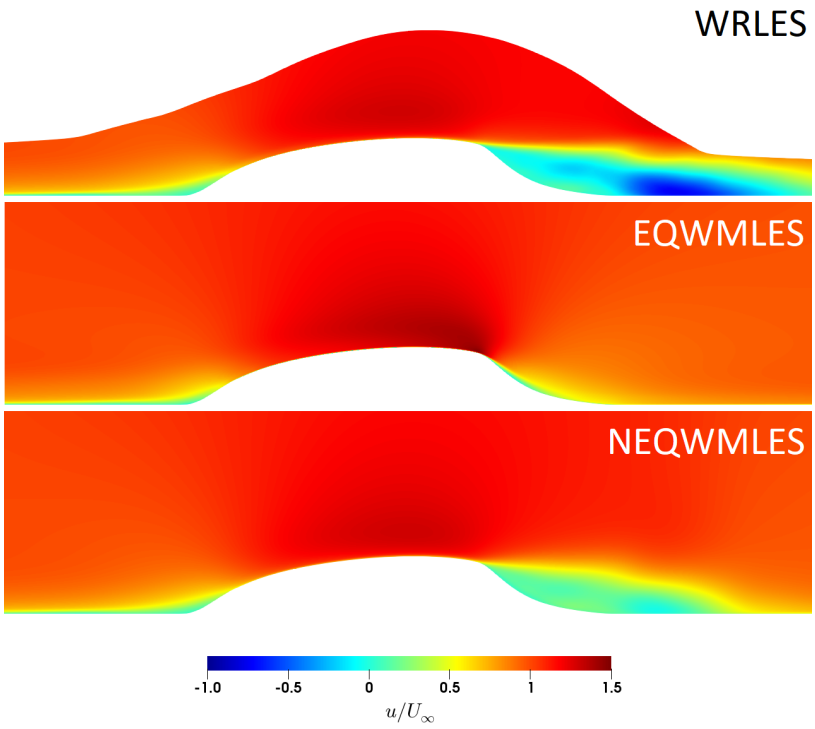

Figure 4.5: Time-averaged streamwise velocity for the wall mounted hump. For the WRLES results, only the structured grid region is shown.

recirculation region were underpredicted by the NEQWM. Additionally, the thickening of the boundary layer forward of the hump was better predicted with the NEQWM.

The time-averaged streamwise skin friction coefficient for the wall resolved and wall modeled approaches is shown in Figure 4.6. The initial increase in the skin friction coefficient at the leading edge of the hump as a result of the favorable pressure gradient was captured well by both models, but the EQWM severely underpredicted the peak and showed a near-constant skin friction over the hump from $x/c = 0.1$ to the separation point. In contrast, the NEQWM predicted the skin friction in good agreement with the WRLES results until $x/c = 0.2$, where the inflection and decrease of the WRLES skin friction profile were not captured. However, the average magnitude of the skin friction was predicted well by the NEQWM over the entire hump. In the region prior to the separation point, the NEQWM underpredicted the skin friction coefficient by roughly a factor of 10%, in comparison to a 30-50% underprediction by the EQWM. Both models showed a sharp decrease in the

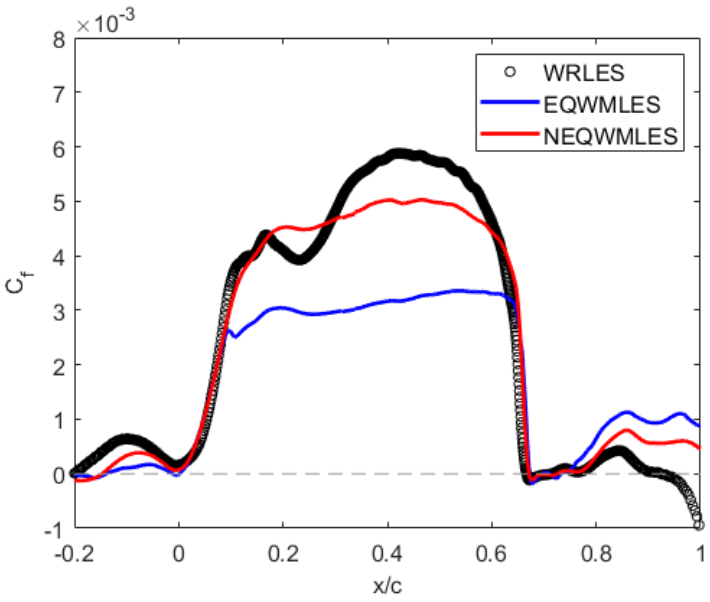

Figure 4.6: Time-averaged streamwise skin friction coefficient for the wall mounted hump.

skin friction at the separation point in good agreement with the WRLES results, but poor predictions were observed with both models in the recirculation region, with the NEQWM performing slightly better in that aspect.

A comparison of the time-averaged pressure coefficient for the three approaches is shown in Figure 4.7. Prior to the separation point, the pressure coefficient distribution was predicted well by both the EQWM and NEQWM in comparison to the WRLES results, with some slight overprediction in magnitude by the EQWM aft of the half chord. The increase in the pressure coefficient at the separation point was also predicted well by both models without notable differences between the two. In the recirculation region, the pressure coefficient was slightly overpredicted in magnitude by both models.

The streamwise velocity profiles at cross-sections $x/c = 0.5$, 0.8, and 1.0 are shown in Figure 4.8. At $x/c = 0.5$, there was excellent agreement in the velocity profile between the WRLES and NEQWMLES results. An overshoot in the velocity profile of the EQWMLES was observed as a result of the increased boundary layer momentum due to an underprediction in the wall shear stress in the region of favorable pressure gradients. At $x/c = 0.8$, the WRLES results showed reversed flow in the velocity profile. The inflection of this velocity

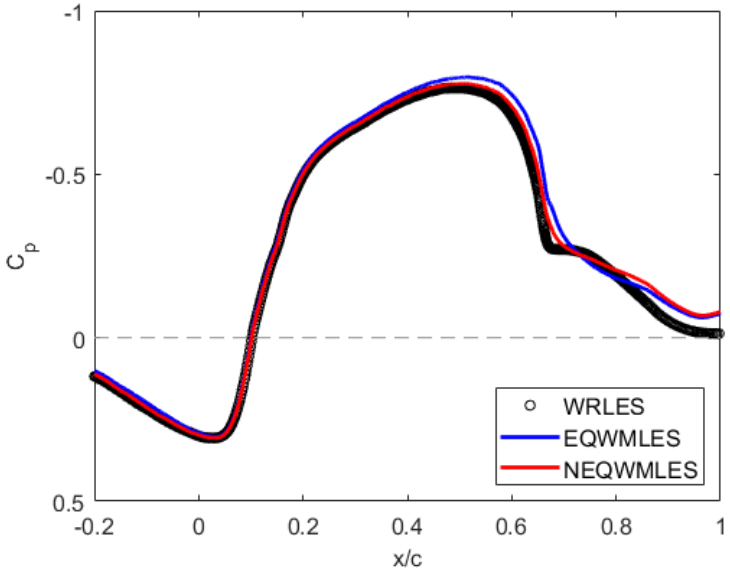

Figure 4.7: Time-averaged pressure coefficient for the wall mounted hump.

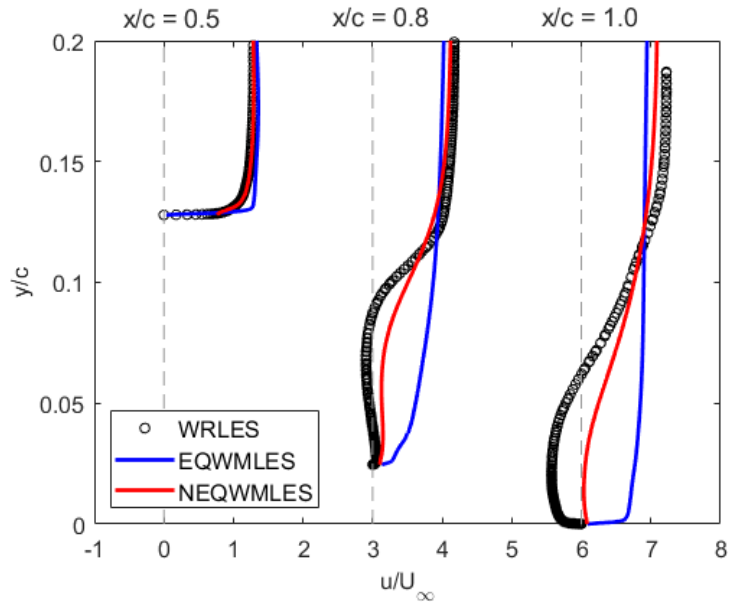

Figure 4.8: Time-averaged streamwise velocity profiles for the wall mounted hump at $x/c = 0.5$, 0.8, and 1.0. Profiles are shifted by 0, +3, +6 along the abscissa, respectively.

profile was captured by the NEQWM, but the magnitude was underpredicted and no flow reversal was observed. Similar observations occurred at $x/c = 1.0$. In comparison, the EQWM did not predict any inflection or flow reversal at both locations, and the velocity profile remained as one of an attached flow.

4.3 Iced Airfoil

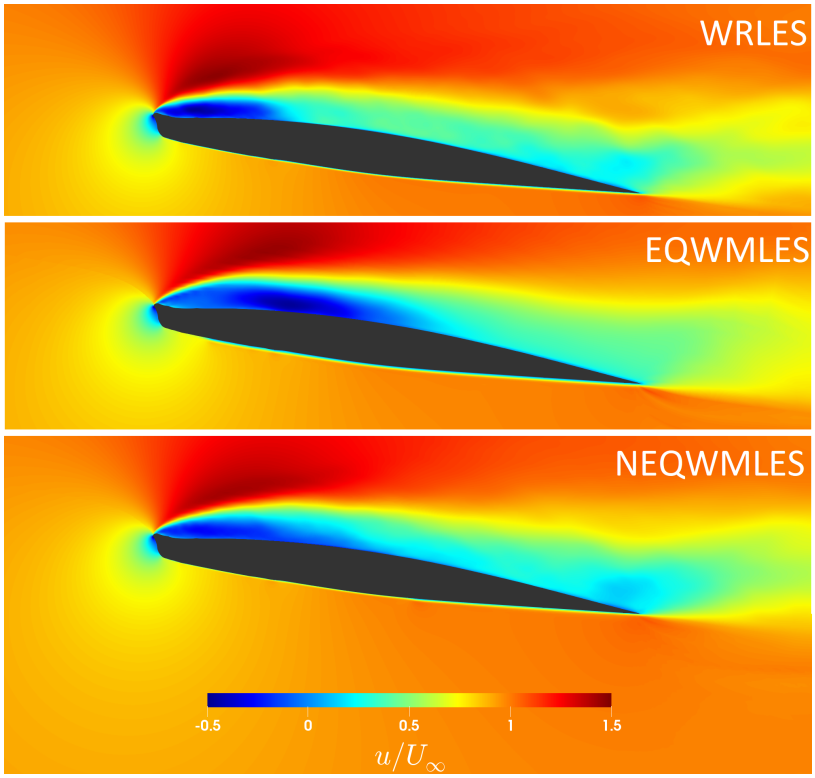

Figure 4.9: Time-averaged chordwise velocity for the iced airflow.

The time-averaged chordwise velocity field for the iced airfoil as predicted by the WRLES, EQWMLES, and NEQWMLES methods is shown in Figure 4.9. The WRLES results showed highly-separated flow along the upper surface of the airfoil with a recirculation region from the leading edge to roughly one-third chord. Both wall models predicted the separation at the leading edge but the extent and height of the recirculation region varied. The EQWMLES approach overpredicted the height and extent of the recirculation region, whereas the NEQWMLES approach predicted the height similarly to the EQWMLES ap-

proach but the extent was in better agreement with the WRLES results. Along the lower surface, the EQWMLES results showed significant thickening of the boundary layer near the leading edge that was not evident in the WRLES results. In contrast, the boundary layer thickening was not evident in the NEQWMLES results which suggests that the NEQWM performs better in laminar flows as it can account for the effects of pressure gradients.

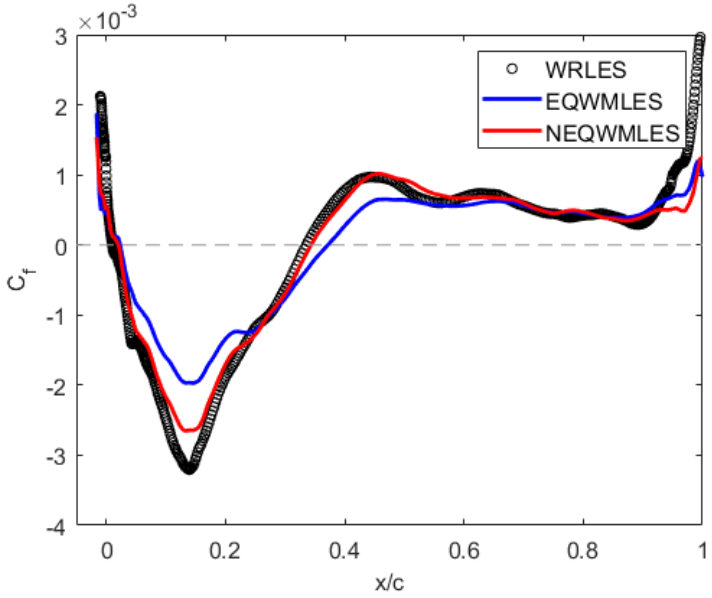

Figure 4.10: Time-averaged chordwise skin friction coefficient for the upper surface of the iced airfoil.

A comparison of the time-averaged chordwise skin friction coefficient of the iced airfoil for the wall resolved and wall modeled approaches is shown in Figures 4.10 and 4.11. Along the upper surface of the airfoil, the recirculation region is evident since the skin friction coefficient is negative near the leading edge. The skin friction in this recirculation region and aft of the reattachment point was predicted well by the NEQWM, although the peak of the reversed flow was slightly underpredicted. The EQWM underpredicted the peak of the reversed flow by roughly a factor of 40%, and the skin friction profile near the reattachment point was in poor agreement with the WRLES results. The location of the reattachment point was predicted very well by the NEQWM, whereas the EQWM predicted the reattachment roughly 5% of a chord length aft of the WRLES results. Along the laminar

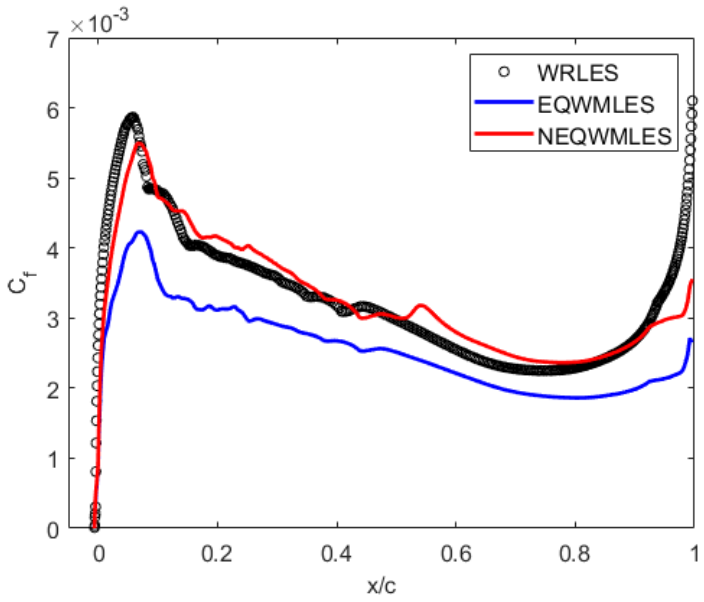

Figure 4.11: Time-averaged chordwise skin friction coefficient for the lower surface of the iced airfoil.

lower surface, the NEQWMLES results were in good agreement with the WRLES results since the effects of pressure gradients on the wall shear stress were included while the EQWM underpredicted the skin friction by 10 to 20% along the entire surface. For both models, the rise in skin friction at the trailing edge was not predicted well, suggesting that the chordwise grid spacing was too coarse to resolve the trailing edge effects.

The time-averaged pressure coefficient along the iced airfoil is shown in Figure 4.12. Along the upper surface prior to the reattachment point, the pressure coefficient was better predicted with the NEQWM than the EQWM. The suction peak was underpredicted by roughly 10% by both models, but the rise in pressure aft of the suction peak predicted by the NEQWM was in better agreement with the WRLES results than the prediction by the EQWM. Aft of the reattachment point, both models predicted the pressure coeefficient in good agreement with the WRLES results. Along the lower surface, the pressure coefficient distribution of the EQWMLES and NEQWMLES results were nearly identical and in good agreement with the pressure distribution of the WRLES results.

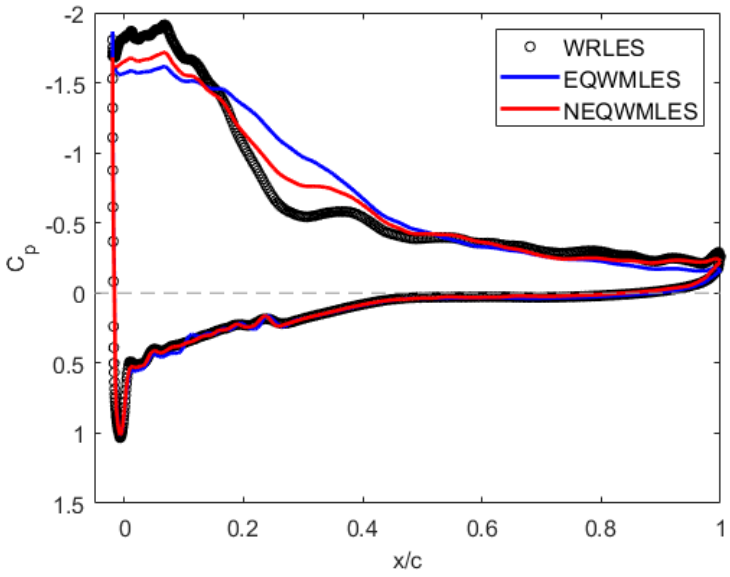

Figure 4.12: Time-averaged pressure coefficient for the iced airfoil.

4.4 Computational Cost

A comparison of the computational costs of the three approaches in core hours per flow over chord and percent increase over the minimum is shown in Table 4.1. The computational cost of GPU solving was approximated in CPU core hours by assuming half of the peak performance of the GPU, resulting in approximately 1,720 core hours per GPU hour.

	Wall Mounted Hump		**Iced Airfoil**	
WRLES	160,290	+ 1878 %	7,120	+ 1530 %
EQWMLES	8,108	-	437	-
NEQWMLES	8,824	+ 9 %	460	+ 5%

Table 4.1: Computational cost in CPU core hours per flow over chord of the WRLES, EQWMLES, and NEQWMLES approaches.

Between the wall resolved and wall modeled approaches, the computational cost increased by a factor of 15 to 20. Although theoretically the NEQWM should have the same computational cost as the EQWM, a cost increase of 5 to 10% was observed, which can be attributed to the NEQWM equations taking longer to converge. This increase can be reduced with the implementation of more elaborate ODE solvers. In comparison, non-

equilibrium wall models that include the time derivative can have a computational cost multiple times that of an equilibrium wall model.

CHAPTER 5
CONCLUSION

For high Reynolds number flows, wall modeling is essential for performing large eddy simulation at a reasonable computational cost. In this work, the method of wall shear stress modeling was explored. For this approach, the treatment of the pressure gradient, convective, and time derivatives dictates the category for which the wall shear stress model falls under. Equilibrium wall models neglect these terms while non-equilibrium wall models incorporate these terms. The assumptions used by equilibrium wall models to neglect these terms result in accurate predictions for many types of flows. However, for flows with strong separation and laminar regimes, these assumptions do not hold, and therefore non-equilibrium are more applicable for a broader range of flows, albeit at a significant increase in computational cost and complexity.

The computational cost and complexity of TBLE-based non-equilibrium models can be attributed to two terms: the wall parallel gradients and the time derivative. The former requires an embedded resolved grid within the LES grid, which leads to significant additional complexity in implementation and usage for complex geometries. The latter requires that the wall model equations be treated as a time-stepping initial value problem (IVP) to resolve the fluctuations of the wall model solution over time and to maintain physical consistency with the Lagrangian nature of fluid accelerations, which results in maximum time step restrictions for the LES solver to maintain stability in the wall model solution.

In this work, a novel ODE-based non-equilibrium wall model was introduced that does not require the solution of either the time derivative or the wall parallel gradients within the wall model. An approximate form of the pressure gradient and convective terms was used as to not require an embedded wall model grid. The approximation of the convective and pressure gradient terms was generated with a polynomial interpolation of the LES solution

within the wall model region. Expanding upon the work of Hickel *et al.*, the introduction of an approximation error for the convective term profile was removed by enforcing matching to the convective term of the LES solver at the wall model height. The effects of the polynomial interpolation order on the accuracy of the wall model were explored and a linear profile was deemed to be sufficient as higher-order approximations did not yield any discernible differences.

As a result of the spatial decoupling of the wall model equations due to the approximation of the wall parallel gradients instead of direct evaluation, a significant saving in computational cost was possible through the solution of the steady form of the wall model equations which could not be done with traditional wall models that evaluate the wall parallel gradients. By neglecting the time derivative, the wall model equations can be solved as a simpler boundary value problem (BVP), but overpredictions in the wall shear stress are observed as the unsteady term acts to damp changes in the velocity field between time steps. Hoffmann and Benocci attempted to model the time derivative by approximating it as a source/sink in the steady BVP formulation of the TBL equations, which yielded good results for attached flows but was ill-posed for separated flows. In contrast to the approach by Hoffmann and Benocci, a model for the effects of the time derivative on the changes in the velocity gradients between time steps was created. The empirically determined model served to reduce the changes in the wall shear stress between time steps as a function of the magnitude of the forcing term approximation within the wall model region. To the author's knowledge, this proposed wall model is the first TBLE based non-equilibrium wall model that does not require the solution of a time-stepping problem without an overprediction in the skin friction for flows with strong non-equilibrium effects. As a result, the proposed model can operate at near identical time step sizes to equilibrium wall models, significantly reducing the computational cost compared to non-equilibrium wall models in the literature.

Wall resolved and wall modeled LES were performed on the NASA wall mounted hump and an iced NACA 63A213 airfoil to assess the proposed wall model in compari-

son to a commonly used equilibrium wall model of Kawai & Larsson for flows with strong non-equilibrium effects. For the wall mounted hump, the proposed non-equilibrium wall model predicted trailing edge separation in much better agreement than the equilibrium wall model which did not show evident signs of separation. However, the extent of the separation region was underpredicted by the non-equilibrium wall model. For the iced airfoil, the extent of the separation region was overpredicted by the equilibrium model whereas the non-equilibrium model predicted it in closer agreement with the wall resolved results. Excellent predictions of the laminar flow region were observed with the non-equilibrium wall model in contrast to the poor performance of the equilibrium wall model in predicting laminar boundary layer effects. Improvements in the skin friction predictions were observed with the non-equilibrium model along the surface of the wall mounted hump and in the laminar and separated flow regions of the iced airfoil, reducing the general underprediction of the equilibrium wall models from 20-40% to less than 10%. Inflections and reversed flow in the velocity profiles for the hump were captured by the non-equilibrium wall model, although underpredicted in comparison to the wall resolved results. No such inflections and reversed flow were shown in the equilibrium wall model results. Minor improvements in the pressure coefficient prediction were also observed. The results suggest that the proposed wall model can offer much better predictions of separated and/or laminar flows compared to equilibrium wall models.

As the non-equilibrium wall model relies on empirically determined coefficients, further tests must be carried out to validate the wall model against flows with varying degrees of non-equilibrium effects. Although the proposed wall model did perform reasonably well for the two test cases, several other types of flows are of interest: (1) equilibrium flows, (2) flows with multiple separation and reattachment points, and (3) transitional flows. The proposed wall model must be validated against equilibrium flows such as a channel or a flat plate to confirm that it reduces to the equilibrium wall model in equilibrium flows. Flows with multiple separation and reattachment points could pose a challenge for the proposed

wall model since the underpredictions of the skin friction and mean velocity observed in separated flow regions could compound into significant inaccuracies. For transitional flows, wall modeled approaches generally yield poor predictions of the near wall behavior. However, it would be beneficial to observe the behavior of the proposed wall model in comparison to an equilibrium wall model in transitional flows and determine if the corrections for transitional flows used by equilibrium models are still suitable. As with any wall modeled approach, the effects of grid dependence must be determined. This is particularly true for the proposed wall model since the grid spacing was not varied except in the wall normal direction between approaches, and the wall normal spacing of the first cell ($y^+ \approx 30$) was essentially identical between the two cases. The effects of wall normal as well as wall parallel grid spacing must be explored to determine the robustness of the time derivative model.

Potential improvements could be gained through better treatment of the individual non-equilibrium terms in the polynomial approximation. For example, V and $\frac{\partial U}{\partial x}$ could be interpolated separately while $\frac{\partial U}{\partial y}$ and U are taken from the wall model solution. Further improvements in the eddy viscosity formulation could be obtained by matching the LES eddy viscosity at the interface location, similar to the work of Wang and Moin [12], or through formulations that result in analytic solutions to the wall model equations. Additionally, the extension of the wall model equations to include the temperature boundary condition as well as the effects of moderate to strong compressibility can be performed. A notable drawback of the proposed wall model is the behavior of the time derivative model in the initial stages of a flow simulation. If the flow within the wall model is in perfect equilibrium (i.e., the pressure and velocity is constant), the reduction factor ζ would be zero and no change in the wall shear stress would happen. Physically, this scenario cannot happen, but it can happen in the start of a numerical simulation. If a simulation is initialized with constant initial conditions and constant inlet for a flow without inviscid gradients (e.g., channel flow), the wall model would predict no wall shear stress and the flow would

not develop. Edge cases such as these must be accounted for in future development and validation of the time derivative model.

REFERENCES

[1] G. Park and P. Moin, "An improved dynamic non-equilibrium wall-model for large eddy simulation," *Physics of Fluids*, vol. 26, pp. 015–108, Jan. 2014.

[2] S. Kawai and J. Larsson, "Dynamic non-equilibrium wall-modeling for large eddy simulation at high reynolds numbers," *Physics of Fluids*, vol. 25, no. 1, pp. 015–105, 2013.

[3] J. Larsson, S. Kawai, J. Bodart, and I. Bermejo-Moreno, "Large eddy simulation with modeled wall-stress: Recent progress and future directions," *Mechanical Engineering Reviews*, vol. 3, pp. 15–41, Nov. 2015.

[4] J. W. Deardorff, "A numerical study of three-dimensional turbulent channel flow at large reynolds numbers," *Journal of Fluid Mechanics*, vol. 41, no. 2, pp. 453–480, 1970.

[5] U. Schumann, "Subgrid scale model for finite difference simulations of turbulent flows in plane channels and annuli," *Journal of Computational Physics*, vol. 18, no. 4, pp. 376–404, 1975.

[6] G. Grotzbach, "Direct numerical and large eddy simulation of turbulent channel flows," *Encyclopedia of Fluid Mechanics*, pp. 1337–1391, 1987.

[7] U. Piomelli, J. Ferziger, P. Moin, and J. Kim, "New approximate boundary conditions for large eddy simulations of wallbounded flows," *Physics of Fluids A: Fluid Dynamics*, vol. 1, no. 6, pp. 1061–1068, 1989.

[8] T.-H. Shih, L. Povinelli, and N. S. Liu, "Application of generalized wall function for complex turbulent flows," *Journal of Turbulence*, vol. 4, pp. 177–186, Apr. 2003.

[9] H. Werner and H. Wengle, "Large-eddy simulation of turbulent flow over and around a cube in a plate channel," in *Turbulent Shear Flows 8*, 1993, pp. 155–168.

[10] X. Wu and K. D. Squires, "Prediction of the three-dimensional turbulent boundary layer over a swept bump," *AIAA Journal*, vol. 36, no. 4, pp. 505–514, 1998.

[11] G. Hoffmann and C. Benocci, "Approximate wall boundary conditions for large eddy simulations," *Advances in Turbulence V*, vol. 24, pp. 222–228, Jan. 1995.

[12] M. Wang, "Les with wall models for trailing-edge aeroacoustics," *Annual Research Briefs, Center for Turbulence Research, Stanford University*, pp. 355–364, 1999.

[13] E. Balaras and C. Benocci, "Subgrid scale models in finite difference simulations of complex wall bounded flows," *Application of Direct and Large Eddy Simulation to Transition and Turbulence*, vol. 6, pp. 06–34, Nov. 1994.

[14] E. Balaras, C. Benocci, and U. Piomelli, "Two-layer approximate boundary conditions for large-eddy simulations," *AIAA Journal*, vol. 34, no. 6, pp. 1111–1119, 1996.

[15] W. Cabot, "Near-wall models in large eddy simulations of flow behind a backward-facing step," *NASA Technical Reports*, 1996.

[16] B. Diurno GV and P. U. E, "Walllayer models for les of separated flows," *Modern Simulation Strategies for Turbulent Flows*, pp. 207–22, 2001.

[17] M. Wang and P. Moin, "Dynamic wall modeling for large-eddy simulation of complex turbulent flows," *Physics of Fluids*, vol. 14, no. 7, pp. 2043–2051, 2002.

[18] S. Hickel, E. Touber, J. Bodart, and J. Larsson, "A parametrized non-equilibrium wallmodel for large-eddy simulation," *8th International Symposium on Turbulence and Shear Flow Phenomena*, pp. 127–136, 2012.

[19] G. Coleman, A. Garbaruk, and P. Spalart, "Direct numerical simulation, theories and modelling of wall turbulence with a range of pressure gradients," *Flow Turbulence and Combustion*, vol. 95, pp. 261–276, Oct. 2015.

[20] I. Bermejo-Moreno, L. Campo, J. Larsson, J. Bodart, D. Helmer, and J. K. Eaton, "Confinement effects in shock wave/turbulent boundary layer interactions through wall-modelled large-eddy simulations," *Journal of Fluid Mechanics*, vol. 758, pp. 5–62, 2014.

[21] F. Tessicini, G. Iaccarino, M. Fatica, M. Wang, and R. Verzicco, "Wall modeling for large-eddy simulation using an immersed boundary method," *Annual Research Briefs, Center for Turbulence Research, Stanford University*, pp. 181–187, 2002.

[22] J Bodart and J Larsson, "Wall-modeled large eddy simulation in complex geometries with application to high-lift devices," *Annual Research Briefs, Center for Turbulence Research, Stanford University*, pp. 37–48, 2011.

[23] S. Bocquet, P. Sagaut, and J. Jouhaud, "A compressible wall model for large-eddy simulation with application to prediction of aerothermal quantities," *Physics of Fluids*, vol. 24, no. 6, pp. 065–103, 2012.

[24] K. M. Aikens, N. S. Dhamankar, C. S. Martha, Y. Situ, G. A. Blaisdell, A. S. Lyrintzis, and Z. Li, "Equilibrium wall model for large eddy simulations of jets for aeroacoustics," *AIAA SciTech 2014 Forum*, Jan. 2014.

[25] Y. Tamaki, Y. Fukushima, Y. Kuya, and S. Kawai, "Large-eddy simulation of airfoil flows at near-stall conditions using equilibrium/non-equilibrium wall models," *AIAA Scitech 2019 Forum*, Jan. 2019.

[26] G. I. Park, "Wall-modeled large-eddy simulation of a high reynolds number separating and reattaching flow," *AIAA Journal*, vol. 55, no. 11, pp. 3709–3721, 2017.

[27] S. Kawai and K. Asada, "Wall-modeled large-eddy simulation of high reynolds number flow around an airfoil near stall condition," *Computers & Fluids*, vol. 85, pp. 105 –113, 2013.

[28] X. Yang, J. Sadique, R. Mittal, and C Meneveau, "Integral wall model for large eddy simulations of wall-bounded turbulent flows," *Physics of Fluids*, vol. 27, pp. 025–112, Feb. 2015.

[29] P. Catalano, M. Wang, G. Iaccarino, and P. Moin, "Numerical simulation of the flow around a circular cylinder at high reynolds numbers," *International Journal of Heat and Fluid Flow*, vol. 24, pp. 463–469, Aug. 2003.

[30] A. Vreman, B. Geurts, and J. Kuerten, "Subgrid-modelling in les of compressible flow," in *Direct and Large-Eddy Simulation I*, ser. Fluid Mechanics and Its Applications, Feb. 1994, pp. 133–144.

[31] A. Favre, "Turbulence: Spacetime statistical properties and behavior in supersonic flows," *The Physics of Fluids*, vol. 26, no. 10, pp. 2851–2863, 1983.

[32] J. Smagorisnky, "General circulation experiments with the primitive equations," *Monthly Weather Review*, vol. 91, no. 3, pp. 99–164, 1963.

[33] M. Germano, U. Piomelli, P. Moin, and W. H. Cabot, "A dynamic subgrid-scale eddy viscosity model," *Physics of Fluids A: Fluid Dynamics*, vol. 3, no. 7, pp. 1760–1765, 1991.

[34] C. Duprat, G. Balarac, O. Mtais, P. M. Congedo, and O. Brugire, "A wall-layer model for large-eddy simulations of turbulent flows with/out pressure gradient," *Physics of Fluids*, vol. 23, no. 1, pp. 015–101, 2011.

[35] R. L. Simpson, "A model for the backflow mean velocity profile," *AIAA Journal*, vol. 21, no. 1, pp. 142–143, 1983.

[36] M. Manhart, N. Peller, and C. Brun, "Near-wall scaling for turbulent boundary layers with adverse pressure gradient," *Theoretical and Computational Fluid Dynamics*, vol. 22, no. 3, pp. 243–260, 2008.

[37] D. Greenblatt, K. B. Paschal, C. S. Yao, J. Harris, N. W. Schaeffler, and A. E. Washburn, "Experimental investigation of separation control part 1: Baseline and steady suction," *AIAA Journal*, vol. 44, no. 12, pp. 2820–2830, 2006.

[38] A. M. DeGennaro, C. W. Rowley, and L. Martinelli, "Uncertainty quantification for airfoil icing using polynomial chaos expansions," *Journal of Aircraft*, vol. 52, no. 5, pp. 1404–1411, 2015.

[39] F. Witherden, A. Farrington, and P. Vincent, "Pyfr: An open source framework for solving advectiondiffusion type problems on streaming architectures using the flux reconstruction approach," *Computer Physics Communications*, vol. 185, no. 11, pp. 3028–3040, 2014.

[40] P. L. Roe, "Characteristic-based schemes for the euler equations," *Annual Review of Fluid Mechanics*, vol. 18, no. 1, pp. 337–365, 1986.

[41] B. Cockburn and C. Shu, "The local discontinuous galerkin method for time-dependent convection-diffusion systems," *SIAM J. Numer. Anal.*, vol. 35, no. 6, pp. 2440–2463, 1998.